



ARTICLE

EGFR-RAS-MAPK signaling is confined to the plasma membrane and associated endorecycling protrusions

Sachin Surve, Simon C. Watkins , and Alexander Sorkin 

The subcellular localization of RAS GTPases defines the operational compartment of the EGFR-ERK1/2 signaling pathway within cells. Hence, we used live-cell imaging to demonstrate that endogenous KRAS and NRAS tagged with mNeonGreen are predominantly localized to the plasma membrane. NRAS was also present in the Golgi apparatus and a tubular, plasma-membrane derived endorecycling compartment, enriched in recycling endosome markers (TERC). In EGF-stimulated cells, there was essentially no colocalization of either mNeonGreen-KRAS or mNeonGreen-NRAS with endosomal EGFR, which, by contrast, remained associated with endogenous Grb2-mNeonGreen, a receptor adaptor upstream of RAS. ERK1/2 activity was diminished by blocking cell surface EGFR with cetuximab, even after most ligand-bound, Grb2-associated EGFRs were internalized. Endogenous mCherry-tagged RAF1, an effector of RAS, was recruited to the plasma membrane, with subsequent accumulation in mNG-NRAS-containing TERCs. We propose that a small pool of surface EGFRs sustain signaling within the RAS-ERK1/2 pathway and that RAS activation persists in TERCs, whereas endosomal EGFR does not significantly contribute to ERK1/2 activity.

Introduction

RAS proteins are membrane-bound small GTPases that act as molecular switches and cycle between GDP-bound inactive and GTP-bound active forms (reviewed in [Simanshu et al., 2017](#)). The human genome encodes four isoforms of RAS (HRAS, KRAS4A, KRAS4B, and NRAS) transcribed from three RAS genes (*HRAS*, *KRAS*, and *NRAS*, respectively). RAS proteins share a high degree of sequence homology and display redundant functionality with respect to their ability to transform various cell types and activate similar downstream effectors ([Omerovic et al., 2008](#)). However, RAS proteins also display isoform-specific functions characterized by differential subcellular localization, repertoire, and strength of effector interactions; expression patterns in mouse tissues; and contribution during mouse embryogenesis ([Castellano and Santos, 2011](#); [Hood et al., 2019](#); [Johnson et al., 1997](#); [Karnoub and Weinberg, 2008](#); [Terrell et al., 2019](#); [Umanoff et al., 1995](#); [Yan et al., 1998](#)). *KRAS* and other RAS species are mutated in ~30% of cancers and are considered to be major drivers of tumorigenesis ([Prior et al., 2020](#)).

RAS proteins are the principal components of MAPK/extracellular receptor-stimulated kinase 1/2 (ERK1/2) and phosphoinositide-3-phosphate kinase signaling pathways, which control cell proliferation, differentiation, survival, and migration ([Karnoub and Weinberg, 2008](#)). Activation of the RAS-ERK1/2

2 signaling pathway by the EGF receptor (EGFR) is one of the most studied signaling processes and is well understood at both molecular and biochemical levels ([Lemmon and Schlessinger, 2010](#)). Upon EGFR activation, an SH2 adaptor, Grb2, complexed with RAS guanine nucleotide exchange factors, SOS1 and SOS2, is recruited to the receptor, which leads to increased GTP loading of RAS. GTP-RAS recruits RAF kinases to the membrane and activates them, which in turn results in the sequential activation of downstream kinases, MEK1/2 and ERK1/2 ([Widmann et al., 1999](#)). Ligand-activated EGFR is rapidly internalized and accumulates in early/sorting endosomes. Whether endosomal EGFR triggers signaling through the RAS-ERK1/2 pathway and whether such signaling is necessary for sustained ERK1/2 activation is unclear. Strong evidence exists for the presence of EGFR-Grb2 complexes in endosomes ([Di Guglielmo et al., 1994](#); [Fortian and Sorkin, 2014](#); [Oksvold et al., 2000](#)). At the same time, analyses of the effects of endocytosis inhibitors on EGF-induced activation of the RAS-ERK1/2 pathway produced contrasting results ([DeGraff et al., 1999](#); [Galperin and Sorkin, 2008](#); [Johannessen et al., 2000](#); [Roy et al., 2002](#); [Sousa et al., 2012](#); [Teis et al., 2002](#); [Vieira et al., 1996](#); [Whistler and von Zastrow, 1999](#)), and the role of endocytic trafficking in signaling through the RAS-ERK1/2 axis remains under debate.

Department of Cell Biology, University of Pittsburgh School of Medicine, Pittsburgh, PA.

Correspondence to Alexander Sorkin: sorkin@pitt.edu.

© 2021 Surve et al. This article is distributed under the terms of an Attribution-Noncommercial-Share Alike-No Mirror Sites license for the first six months after the publication date (see <http://www.rupress.org/terms/>). After six months it is available under a Creative Commons License (Attribution-Noncommercial-Share Alike 4.0 International license, as described at <https://creativecommons.org/licenses/by-nc-sa/4.0/>).

RAS is the most receptor-distal membrane component of this signaling pathway, and therefore defining the membrane compartment(s) where RAS is localized and activated is key to understanding the spatiotemporal regulation of this pathway. RAS proteins contain membrane-targeting determinants in their C-terminal hypervariable regions (HVRs; reviewed in [Prior and Hancock, 2012](#)). The CAAX motif (cysteine [C], two aliphatic amino acids [AA], and other terminal amino acids [X]) in HVR of all RAS isoforms is farnesylated. Two or one cysteines in, respectively, HRAS and NRAS are palmitoylated, probably in the Golgi apparatus, which facilitates their targeting to the plasma membrane. KRAS4B is not palmitoylated, and its targeting to the plasma membrane is mediated by the interaction of the polybasic region in HVR with negatively charged phospholipids. In addition to the plasma membrane, RAS has been detected on endosomes, including those containing EGFR and Grb2 ([Jiang and Sorkin, 2002](#); [Lu et al., 2009](#); [Pol et al., 1998](#)), Golgi ([Chiu et al., 2002](#)), ER ([Bivona and Philips, 2003](#); [Chiu et al., 2002](#)), and even mitochondria ([Bivona et al., 2006](#); [Wolfman et al., 2006](#)). However, the vast majority of studies have used plasmid-mediated transfection and hence overexpression methods to study localization of RAS and its mutants. Minimal information is available regarding the subcellular localization of endogenous RAS proteins in living cells ([Pinilla-Macua et al., 2016](#)).

Tagging endogenous proteins using gene editing has been shown to be the optimal approach for studying subcellular localization dynamics of any protein in living cells. Previously, we found that, in contrast to systems where recombinant HRAS was overexpressed, endogenous HRAS was not present in EGFR-containing endosomes ([Pinilla-Macua et al., 2016](#)). Given different mechanisms of membrane targeting of RAS isoforms, in the present study, we analyzed the subcellular localization of endogenous KRAS and NRAS tagged with mNeonGreen fluorescent protein (mNG) using CRISPR/Cas9 gene editing. Live-cell imaging revealed the predominant localization of KRAS and NRAS to be at the plasma membrane, as well as the presence of NRAS in tubular compartments protruding from the plasma membrane to the pericentriolar juxta-Golgi area and a dramatic segregation of EGFR complexed with endogenous fluorescently labeled Grb2 in vesicular endosomes separate from both the RAS proteins in EGF-stimulated cells. The persistent EGF-induced recruitment of Grb2 to the plasma membrane and the sensitivity of ERK1/2 activity to blocking the cell surface EGFR suggested that the activity of the RAS-ERK pathway is sustained by a small pool of surface EGFR, which is demonstrated by EGF-induced translocation of the endogenous fluorescently labeled RAF1 to the plasma membrane and its tubular protrusions.

Results

Generation and characterization of HeLa cells expressing endogenous mNG-KRAS and mNG-NRAS

To study the subcellular localization of endogenous KRAS and NRAS, these proteins were tagged with mNG at their amino-termini using the CRISPR/Cas9 gene-editing method in HeLa cells ([Fig. 1 A](#)). This subclone of HeLa cells was previously used

in our studies of the localization dynamics of other components of the EGFR-ERK1/2 signaling pathway ([Fortian and Sorkin, 2014](#); [Galperin and Sorkin, 2008](#); [Pinilla-Macua et al., 2016](#); [Surve et al., 2019](#)). The insertion of mNG into KRAS and NRAS genes was evident by the presence of mNG fusion proteins and the absence of untagged KRAS and NRAS in two clones of HeLa/mNG-KRAS and HeLa/mNG-NRAS cells ([Fig. 1, B and C](#); also see PCR in [Fig. S1, A and B](#)). Furthermore, sequencing of the regions around the insertion sites showed that there were no unwanted indels, and the intact reading frame was maintained in clones from both edited cell lines. Some gene-edited clones showed slightly higher expression of mNG-KRAS on Western blots as compared with KRAS in parental cells ([Fig. 1, B and C](#)). Such increased expression, previously observed with endogenous gene-edited HRAS ([Pinilla-Macua et al., 2016](#)), is likely attributed to an increased stability of amino-terminally tagged RAS proteins or an altered translation rate. All gene-edited clones expressed EGFR at the cell surface at levels compared with those in parental cells ([Fig. S1 D](#)). Importantly, the kinetics of ERK1/2 activation by EGF (4 ng/ml) in gene-edited cells was essentially similar to that in parental cells ([Figs. 1 D and S1 C](#)), indicating that increased expression of endogenous mNG-KRAS did not affect signal transduction along the EGFR-ERK1/2 pathway. Altogether, the data in [Figs. 1 and S1](#) validated the use of gene-edited cell lines for studying the localization dynamics of endogenous KRAS and NRAS.

mNG-KRAS and mNG-NRAS are predominantly located on the plasma membrane

Live-cell 3D imaging using a spinning-disk confocal microscope demonstrated that mNG-KRAS and mNG-NRAS are localized to the plasma membrane, often present in filopodia, ruffles, and lamellipodia ([Fig. 1 E](#)). mNG-NRAS was additionally seen concentrated in the juxtannuclear region and, in some cells, in diffraction-limited tubular structures ([Fig. 1 E](#)). mNG-KRAS and mNG-NRAS fluorescence was also detected in vesicular compartments throughout the cell periphery and in the perinuclear area. To estimate the fraction of cellular mNG-tagged RAS proteins associated with the plasma membrane, the cells were stained with CellMask Deep Red Plasma Membrane Stain (henceforth called “CellMask”) at RT (20–22°C) or 4°C for 3–45 min to label the plasma membrane and minimize constitutive endocytosis of CellMask-labeled membranes ([Fig. 1 E](#)). Quantification of mNG colocalization with CellMask revealed that at least 70–75% of total cellular mNG-NRAS and mNG-KRAS is located on the plasma membrane ([Fig. 1 F](#)).

Vesicles detected with the 488-nm channel were present in mNG-KRAS- and mNG-NRAS-expressing cells ([Figs. 2 and 3](#)). These vesicles frequently contained transiently expressed APPL1 (early endosomes), Rab5 (early and sorting endosomes), Rab7 (late endosomes), and Rab11 and EHD1 (both markers of recycling endosomes). However, using image acquisition parameters for detection of mNG-tagged RAS proteins, vesicles with a similar 488-nm channel fluorescence intensity were seen to be abundant in parental HeLa cells ([Fig. S2](#)). These vesicles were often colabeled with defined endosomal markers ([Fig. S2](#)). A broad-spectrum autofluorescence endemic to endosomes and

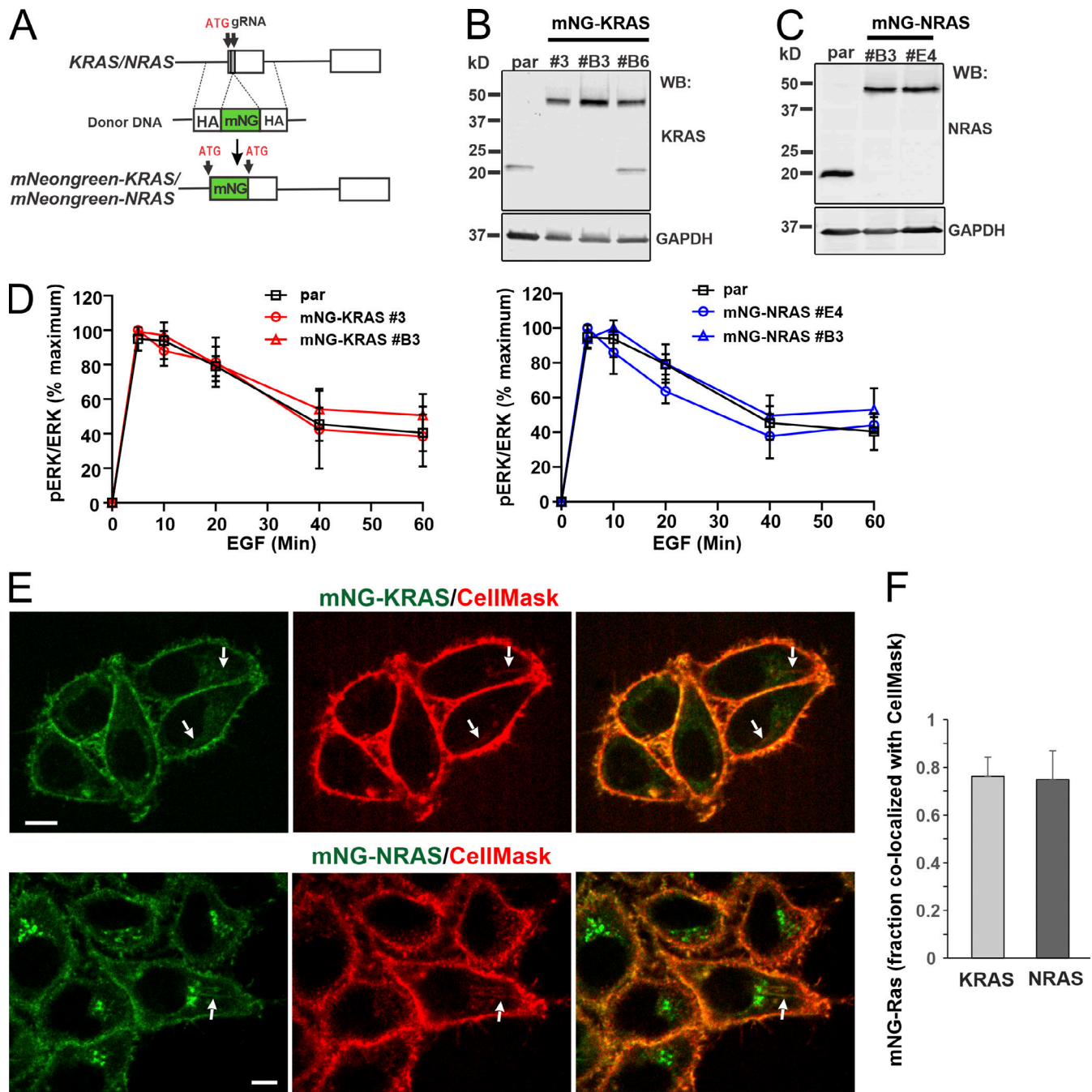


Figure 1. Generation of HeLa/mNG-KRAS and HeLa/mNG-NRAS cells and predominant plasma membrane localization of mNG-KRAS and mNG-NRAS in these cells. (A) Schematics of the insertion of the mNG sequence into the endogenous locus in *KRAS* and *NRAS* genes. See details in Materials and methods. **(B)** Lysates of parental (par) HeLa and single-cell clones of HeLa/mNG-KRAS cells were probed by Western blotting (WB) with KRAS and GAPDH (loading control) antibodies. **(C)** Lysates of parental HeLa and single-cell clones of HeLa/mNG-NRAS cells were probed by Western blotting with NRAS and GAPDH (loading control) antibodies. **(D)** Parental HeLa cells and clones of HeLa/mNG-KRAS and HeLa/mNG-NRAS cells were serum starved and treated with 4 ng/ml EGF for the indicated times at 37°C. Cell lysates were electrophoresed and probed by Western blotting with antibodies to phospho-ERK1/2 (pERK) and ERK1/2. Examples of blots are shown in Fig. S1. The values of the ratios of pERK1/2 to total ERK1/2 were normalized to maximal values of the ratio in each time course and plotted against time. The data on the graph plots are mean values with SEMs from three independent experiments. **(E)** HeLa/mNG-KRAS and HeLa/mNG-NRAS cells were stained with CellMask at RT for 13 min or 4°C for 6 min, respectively. Live-cell imaging was performed through 488-nm (green; mNG) and 640-nm (red; CellMask) channels. Individual confocal sections are shown. Arrows point to examples of tubular shaped compartments. Scale bars, 10 μ m. **(F)** Quantification of the fraction of total cellular mNG-KRAS and mNG-NRAS colocalized with CellMask from images in E. Images of cells incubated with CellMask for 3–13 min at RT or for 3–35 min at 4°C without detectable endocytosis of CellMask were used for quantification. Mean values with SDs are shown ($n = 12$ for mNG-KRAS and $n = 20$ for mNG-NRAS).

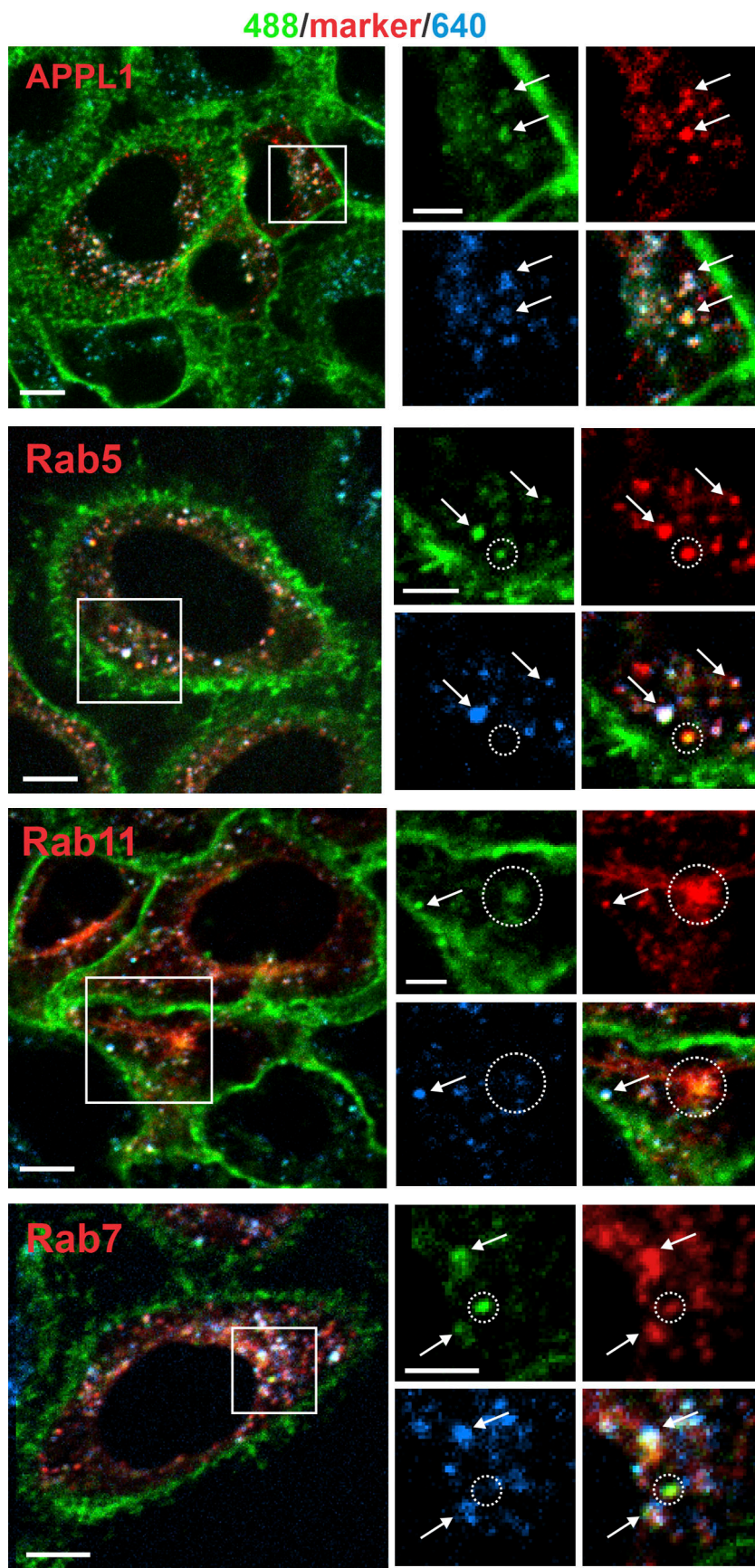


Figure 2. Live-cell imaging of mNG-KRAS and endosomal markers. HeLa/mNG-KRAS cells were transfected with plasmids expressing mRFP-APPL1, mRFP-Rab5, CFP-Rab7, and mCh-Rab11. 3 d after transfection, the cells were imaged through 488-nm (green), 561-nm (red; mRFP and mCh), 445-nm (red; CFP), and 640-nm (blue; auto-fluorescence) channels. Merged-channel maximum-intensity z-projections of two or three consecutive confocal images are presented. Insets represent high-magnification split-channel images of the regions marked by white rectangles. White circles indicate vesicles with 488-nm channel and endosomal marker fluorescence but lacking significant 640-nm channel fluorescence (apparent specific colocalization). Arrows point to examples of vesicles with signals from all three channels (apparent nonspecific colocalization). Auto-fluorescence through 561-nm and 445-nm channels was negligible with image acquisition parameters used for detection of the endosomal markers; therefore, fluorescence through these channels is considered to be specific. Scale bars are 10 μm and 5 μm in full images and insets, respectively.

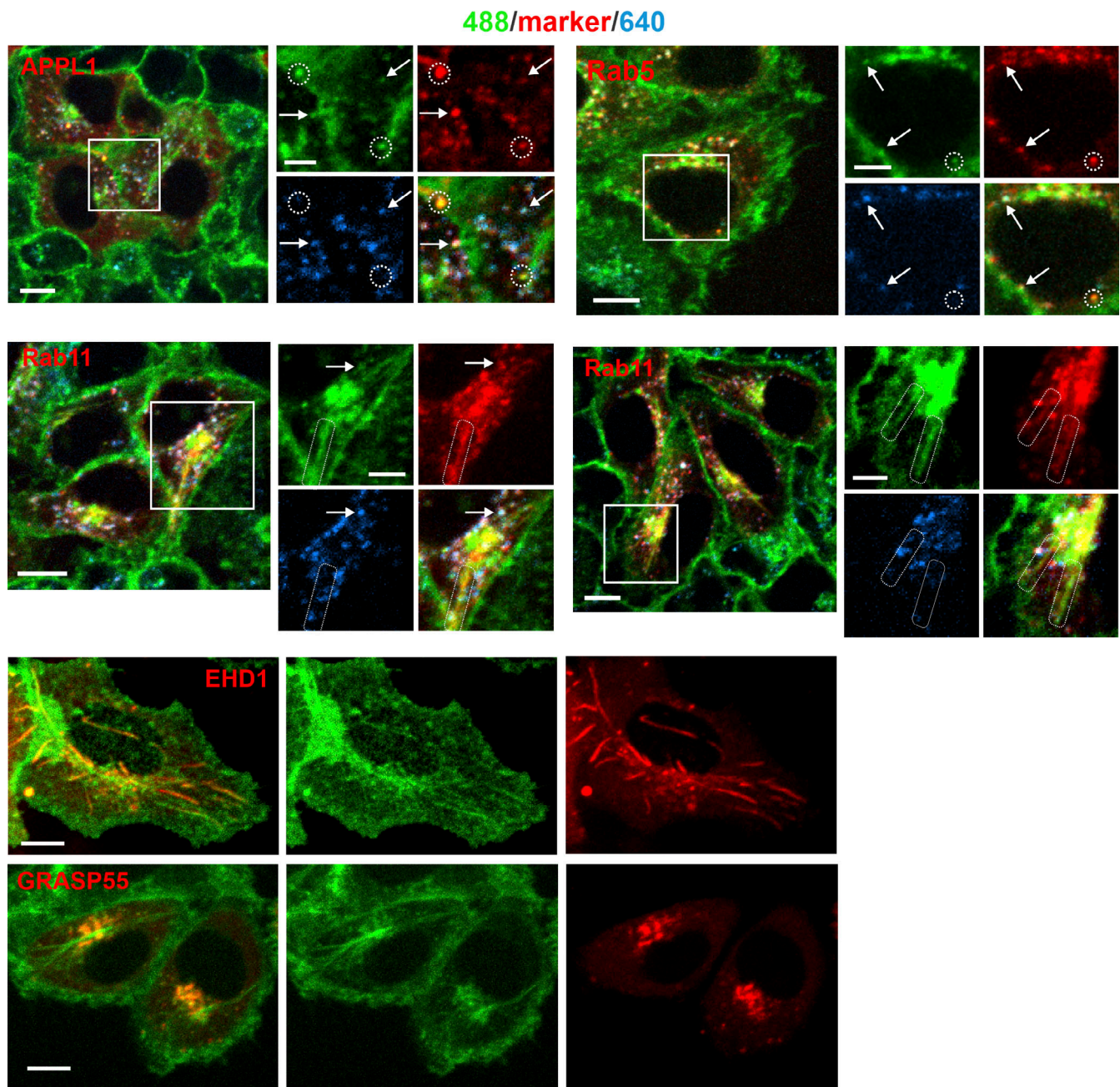


Figure 3. Live-cell imaging of mNG-NRAS and endosomal markers. HeLa/mNG-NRAS cells were transiently transfected with plasmids expressing mRFP-APPL1, mRFP-Rab5, mCh-Rab11, Tomato-EHD1, and GRASP55-mCh. 3 d after transfection, the cells were imaged through 488-nm (green), 561-nm (red; mRFP, Tomato, and mCh), and 640-nm (blue; autofluorescence) channels. Merged-channel maximum-intensity z-projections of two or three consecutive confocal images are presented. Insets represent high-magnification split-channel images of the regions marked by white rectangles. White circles indicate vesicles with 488-nm channel and endosomal marker fluorescence but lacking significant 640-nm channel fluorescence (apparent specific colocalization). Arrows point to examples of vesicles with signals from all three channels (apparent nonspecific colocalization). Tubular structures labeled with mCh-Rab11 and mNG-NRAS are indicated by dashed parallelograms. Autofluorescence through the 561-nm channel was negligible with image acquisition parameters used for detection of endosomal markers; therefore, the fluorescence through this channel is considered to be specific. Scale bars are 10 μ m and 5 μ m in full images and insets, respectively.

lysosomes has been well documented (Tycko et al., 1983). Therefore, to account for this autofluorescence, images of parental and mNG-expressing cells through the 640-nm channel were captured in addition to 488-nm and 561-nm channel images to detect nonspecific fluorescence as performed in our previous studies (Surve et al., 2019). Figs. 2 and 3 show that

many vesicles were detected using both 488-nm and 640-nm channels, suggesting that the vesicular fluorescence detected through the 488-nm channel is likely the autofluorescence rather than specific mNG fluorescence. On rare occasions, however, mNG-KRAS- and mNG-NRAS-labeled vesicles did not emit detectable nonspecific fluorescence through the 640-nm

channel and were colocalized with an endosomal marker (examples shown in Figs. 2 and 3), suggesting that small pools of mNG-KRAS and mNG-NRAS were present in vesicular endosomes. Importantly, plasma membrane and Golgi complex labeled with GRASP55 did not display detectable autofluorescence, as revealed by imaging through the 640-nm channel (Figs. 2 and 3) and other channels in parental cells (Fig. S2). Therefore, plasma membrane and Golgi fluorescence detected with the 488-nm channel in gene-edited cells is considered to be mNG specific.

mNG-NRAS was also frequently localized to diffraction-limited tubular shaped structures, which occasionally extend across the entire cell volume from the cell edge (plasma membrane) to the pericentriolar recycling compartment (PRC) labeled with mCherry (mCh)-Rab11 in the juxta-Golgi area (Fig. 3). These tubules were colabeled with mCh-Rab11 in their PRC-proximal parts and displayed no detectable autofluorescence (Fig. 3). mNG-NRAS was also colocalized with Tomato-EHD1 (Sharma et al., 2009), mainly in the regions of tubules proximal to the plasma membrane, although overexpression of Tomato-EHD1 seemed to have increased membrane tubulation (Fig. 3). Because mNG-NRAS-containing tubular compartments appear to originate at the plasma membrane, we tested whether they are indeed continuous with the plasma membrane by staining with CellMask at low temperature to minimize endocytosis of CellMask-labeled membranes, as performed in Fig. 1 E. As shown in Fig. 4 A, CellMask penetrated into tubular compartments labeled with mNG-NRAS. By contrast, no specific vesicular staining with CellMask was detected in these experiments, confirming negligible endocytic trafficking under temperature-constrained conditions, as would be expected (Fig. 4). CellMask-labeled tubular structures were also detected in mNG-KRAS cells, although mNG-KRAS was typically absent from the structures (Figs. 1 E and 4 B). Moreover, mCh-PH-PLC δ 1, a sensor of phosphoinositol-4,5-bisphosphate (PIP $_2$; Várnai and Balla, 1998), a lipid that is highly enriched in the plasma membrane (Hammond and Burke, 2020), was colocalized with mNG-NRAS not only in cell edges and filopodia-rich membrane but also in the tubular compartments running between the plasma membrane and the Golgi area (Fig. 4 C). In summary, the data in Fig. 4 suggest that mNG-NRAS/Rab11 tubular compartments can indeed be continuous with both the plasma membrane and the PRC. We therefore termed these compartments “tubular endorecycling compartments,” or TERCs.

mNG-KRAS and mNG-NRAS are not detected in EGFR-containing endosomes

To analyze the subcellular localization of endogenous mNG-KRAS and mNG-NRAS during EGF stimulation, the gene-edited and the parental cells were incubated with EGF conjugated to rhodamine (EGF-Rh; 4 ng/ml), and 3D live-cell imaging was performed at 37°C through 488-nm (mNG) and 561-nm channels (EGF-Rh). Autofluorescence was detected by imaging through the 640-nm channel and used for calculation of the nonspecific component of 488-nm channel fluorescence in EGF-Rh-containing endosomes using a spectral unmixing method as previously described (Surve et al., 2019).

EGF-Rh rapidly bound to the cell surface, resulting in both diffuse and clustered distribution after 1–5 min of stimulation and therefore colocalization of EGF-Rh with mNG-KRAS/mNG-NRAS proteins in the plasma membrane (Figs. 5 and 6). This was followed by a robust accumulation of EGF-Rh in vesicular endosomes, such that the plasma membrane fluorescence of EGF-Rh became equivalent to background after 15 min of continuous stimulated endocytosis. At the same time, the pattern of mNG-KRAS and mNG-NRAS localization upon cell stimulation with EGF-Rh did not change, resulting in a clear segregation of the mNG-RAS proteins to the plasma membrane, separate from endosomal EGF-Rh (Figs. 5 and 6). Quantification of the fraction of mNG-KRAS/mNG-NRAS colocalized with EGF-Rh demonstrated an overlap of EGFR and RAS proteins early upon stimulation at the plasma membrane followed by low, if not negligible, levels of their colocalization after ~10 min of continuous EGF-Rh endocytosis (Fig. 7 A).

Although some EGF-Rh-containing endosomes emitted fluorescence through the 488-nm channel (Figs. 5 and 6), virtually all of these endosomes were detectable with the 640-nm channel as well, indicative of substantial autofluorescence in these vesicles. To quantify the specific component of the 488-nm channel fluorescence, the 488 nm/640 nm ratio of nonspecific fluorescence was determined in endosomes of parental HeLa cells stimulated with EGF-Rh. The mean value of this ratio was then used to estimate the nonspecific component of the 488-nm channel fluorescence in endosomes of mNG-KRAS/mNG-NRAS-expressing cells. Subsequent quantification of the specific mNG fluorescence in EGF-Rh-containing endosomes in cells incubated with EGF-Rh for 5–15 min yielded mean values of the mNG/Rh ratio that were not statistically different from the background values measured in parental cells (Fig. 7 B).

To compare the extent of Ras colocalization with EGFR in endosomes relative to other molecules that are accepted to colocalize with EGFR in this compartment, we generated HeLa cells expressing endogenous mNG-labeled Grb2 (Fig. 7 C). Ligand activation of EGFR resulted in rapid recruitment of Grb2-mNG to the plasma membrane followed by dramatic accumulation of EGF-Rh-EGFR-Grb2-mNG complexes in endosomes (Fig. 7 D). The mean value of the mNG/EGF-Rh fluorescence ratio in endosomes of stimulated HeLa/Grb2-mNG cells measured using our spectral unmixing method was ~2.5, which is more than two orders of magnitude larger than values of the mNG-NRAS/EGF-Rh ratio (Fig. 7 B). Together, the data in Fig. 7 demonstrate that endocytosis separates the bulk of EGFR-Grb2 complexes from KRAS and NRAS, which remain primarily at the plasma membrane.

ERK1/2 activity is sustained by signaling from cell surface EGFR and is not affected by the inhibition of endocytosis

We have previously demonstrated that, despite the spatial separation of EGFR from HRAS, sustained signaling through the RAS-MEK-ERK axis requires EGFR kinase activity, and we have proposed that a small number of EGFRs remaining at the plasma membrane continue to signal during the first hour of EGF stimulation (Pinilla-Macua et al., 2016). To further test this hypothesis, the dynamics of the plasma membrane Grb2-mNG

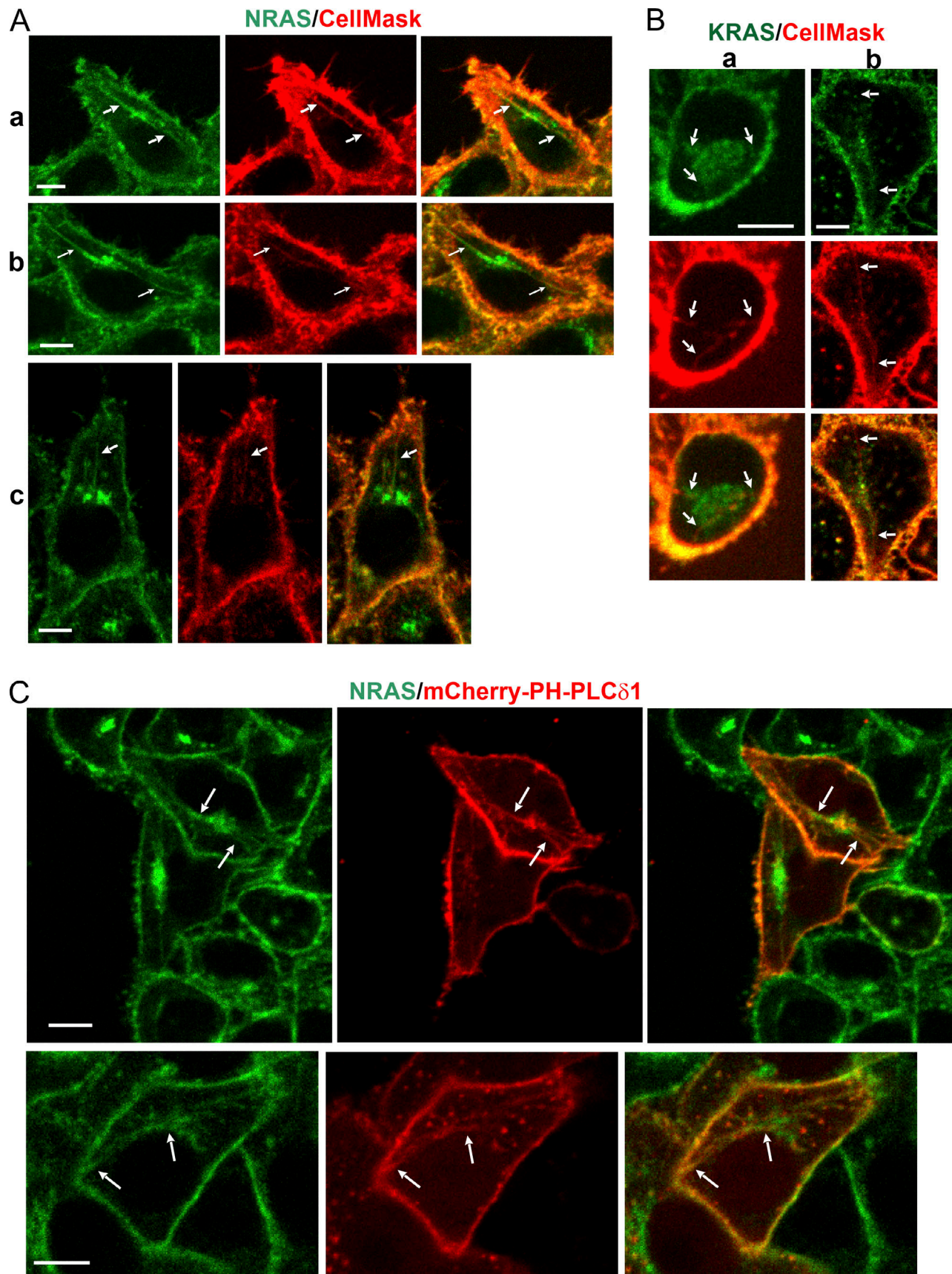


Figure 4. **Detection of CellMask and PIP2 in TERCs in HeLa/mNG-NRAS and HeLa/mNG-KRAS cells.** (A) HeLa/mNG-NRAS cells were stained with CellMask at RT for 8 min (a) or 4°C for 8 min (b) or 21 min (c) and imaged at RT through 488-nm (green; mNG) and 640-nm (red; CellMask) channels. z-Stacks of

images were obtained at 200-nm steps. Maximum-intensity z-projections of two consecutive confocal images are shown. Examples of colocalization of mNG-NRAS and CellMask in TERCs are indicated by arrows. **(B)** HeLa/mNG-KRAS cells were stained with CellMask at 4°C for 15 min (a) and 43 min (b) and imaged as in A. Maximum-intensity z-projections of two consecutive confocal images are shown. Arrows point to a tubular plasma membrane protrusion labeled with CellMask and lacking mNG fluorescence. **(C)** HeLa/mNG-NRAS cells were transfected with the plasmid expressing PIP2 sensor mCh-PLC δ 1. 3 d after transfection, live cells were imaged through 488-nm (green; mNG) and 561-nm (mCh-PLC δ 1) channels. Single confocal sections are shown. Examples of colocalization of mNG-NRAS and PIP2 in TERCs are indicated by arrows. Scale bars, 10 μ m.

were examined by total internal reflection fluorescence (TIRF) microscopy after stimulation with EGF. At basal conditions, Grb2-mNG was detected at the ventral membrane as both small and large puncta, the latter presumably representing focal adhesion complexes (Schlaepfer et al., 1994). EGF caused rapid recruitment of Grb2-mNG to the basal plasma membrane, detected as numerous diffraction-limited puncta, which were most abundant at \sim 5 min and gradually depleted to a level that remained slightly higher than the level observed before EGF stimulation (Fig. 8 B). Importantly, the number of Grb2-mNG puncta was still significantly higher after 15–20 min of EGF stimulation than in unstimulated cells, though this puncta count could have been affected by photobleaching. This observation suggests there is a pool of EGFR–Grb2 complexes that are capable of maintaining RAS activity at the plasma membrane and thus of sustaining ERK1/2 activity beyond the 15-min EGF stimulation.

To directly test whether a small pool of EGFR–Grb2 complexes at the plasma membrane is responsible for sustained ERK1/2 activation, surface EGFRs were blocked by cetuximab, a humanized mouse EGFR mAb that competes with EGF for binding to EGFR and inhibits its downstream signaling (Kawamoto et al., 1983; Mandic et al., 2006; Yoshida et al., 2008). A 15-min cetuximab treatment of parental HeLa cells that had been stimulated with EGF for 5 or 15 min significantly decreased MEK1/2 and ERK1/2 phosphorylation (Fig. 8, C–E), suggesting a major contribution of cell surface EGFR in maintaining MEK1/2 and ERK1/2 activities for at least the first 30 min of EGF stimulation. In parallel experiments, immunofluorescence microscopy revealed that cetuximab binding to cell surface EGFR for 15 min at 37°C results in internalization of \sim 17% receptors as detected by colocalization of cetuximab with early endosomal protein EEA1 (Fig. S3 A), which may serve as part of the mechanism by which cetuximab inhibits EGFR signaling through the RAS–ERK1/2 pathway.

The sensitivity of EGF-induced MEK/ERK activities to cetuximab and the lack of a significant colocalization of RAS with EGFR in endosomes suggest that endocytosis of EGFR may not be the major regulator of this signaling process in HeLa cells. To test whether inhibition of endocytosis affects EGF-induced ERK1/2 activity, the effects of siRNA knockdown of clathrin heavy chain (CHC) and a small-molecule Dyngo-4a, treatments known to inhibit clathrin-mediated endocytosis of EGFR (Huang et al., 2004; Pinilla-Macua and Sorokin, 2015), on the time course of ERK1/2 activation were tested. Both treatments strongly (5–10 times) decreased the initial rate of 125 I-EGF internalization (first 5–20 min) and substantially delayed accumulation of 125 I-EGF in endosomes (Fig. S3, B and C). Neither CHC depletion nor Dyngo-4a significantly altered the kinetics of EGF-dependent ERK1/2

activation, although there was a trend of increased magnitude of ERK1/2 activation at early time points after EGF stimulation in CHC-depleted cells (Fig. 8, F and G). These data further indicate that endocytosis is not essential for signal propagation from EGFR to ERK1/2 and sustained ERK1/2 activation.

Recruitment of RAF1 to the plasma membrane and TERC

To visualize active Ras in EGF-stimulated cells, we tagged RAF1 with mCh by gene editing in cells expressing endogenous mNG-NRAS (Fig. 9 A). Because RAF1 is a low-abundance protein (Shi et al., 2016), detection of endogenous RAF1-mCh required lengthy image acquisition times and high laser power. This resulted in the detection of substantial vesicular autofluorescence through the 561-nm channel that was highly colocalized with vesicles imaged through the nonspecific 640-nm channel, regardless of EGF stimulation (Fig. 9 B). We have previously shown that a small pool of endogenous RAF1 is transiently recruited to the plasma membrane upon EGF stimulation but that RAF1 could be stabilized on the plasma membrane (presumably in a complex with GTP-loaded RAS) in EGF-stimulated cells by RAF inhibitor sorafenib (Surve et al., 2019). Therefore, mNG-NRAS/RAF1-mCh cells were stimulated with EGF in the presence of sorafenib to visualize subcellular localizations of GTP-RAS. Significant EGF-induced accumulation of RAF1-mCh was observed at the plasma membrane (Fig. 9 C; additional examples are presented in Fig. S4). RAF1-mCh was also recruited to TERCs; it was seen in the region of these tubular compartments proximal to cell edges (“peripheral” plasma membrane) as well as in the pericentriolar area (Figs. 9 C and S4). These data directly demonstrate the persistent localization of GTP-loaded RAS at the plasma membrane and the potential activity of intracellular RAS concentrated in TERCs and PRCs.

Discussion

This study is the first quantitative imaging analysis of the localization dynamics of endogenous KRAS and NRAS in living cells. The fundamental goal was to gain a better understanding of the spatiotemporal regulation of the EGFR–RAS–ERK1/2 signaling pathway. We have previously defined the subcellular localization of endogenous HRAS (Pinilla-Macua et al., 2016), but the distinct mechanisms of membrane targeting of RAS species and their nonredundant functions in vivo motivated an unbiased and specific analysis of KRAS and NRAS. Furthermore, development of CRISPR/Cas9 gene-editing methods facilitated generation of fluorescent protein knock-in cell lines, which made it feasible to compare the localization dynamics of endogenous RAS proteins with RAS upstream and downstream components of this signaling pathway, such as Grb2 and RAF1.

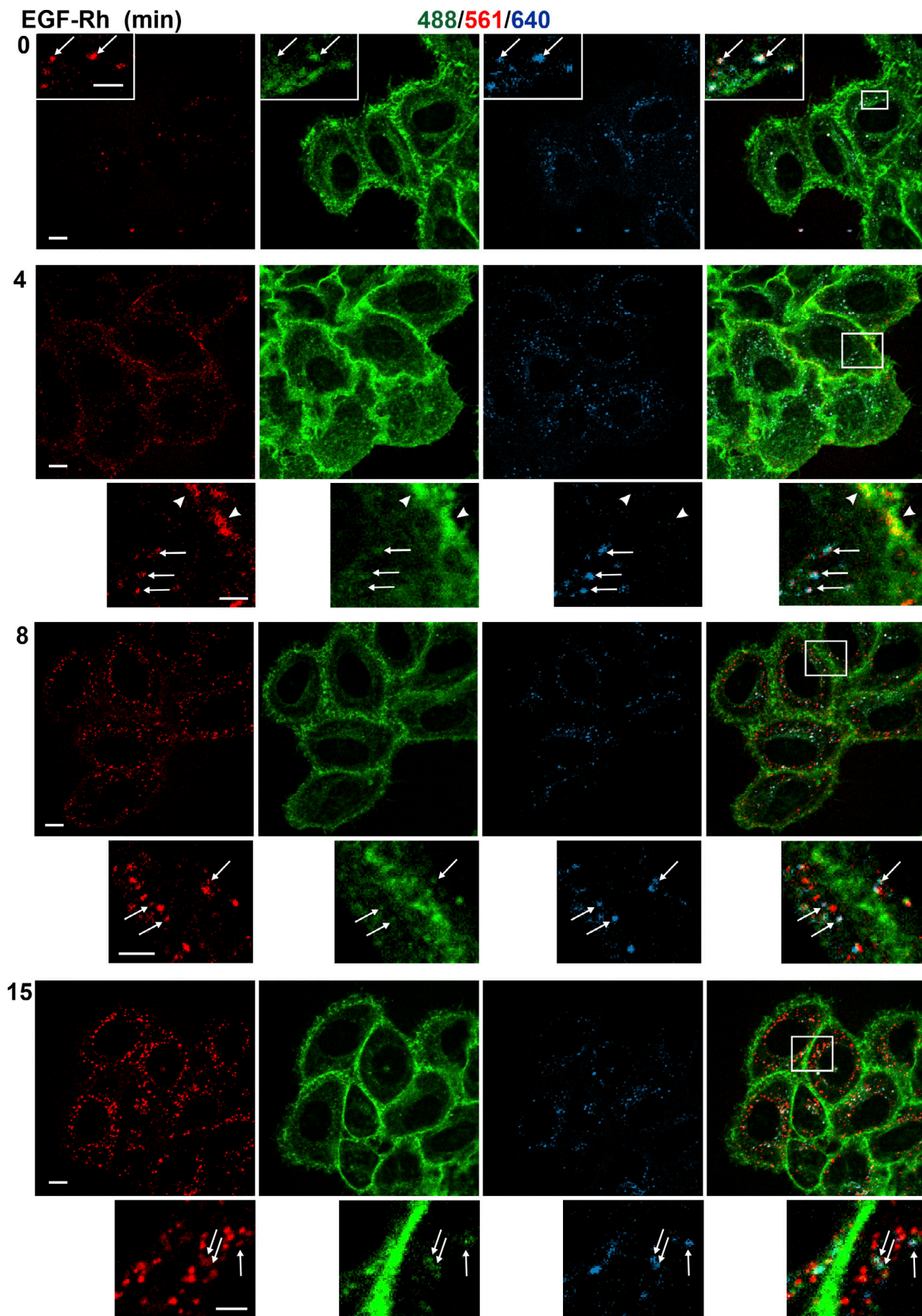


Figure 5. **Localization of mNG-KRAS in EGF-stimulated cells.** HeLa/mNG-KRAS cells were serum starved and treated with 4 ng/ml EGF-Rh at 37°C for the indicated times. 3D live-cell imaging was performed through 488-nm (green), 561-nm (red), and 640-nm (blue; autofluorescence) channels. Fluorescence

intensity scales are identical for full-size images at all time points. Individual confocal sections are shown. Insets are the high-magnification/contrast images corresponding to the regions indicated by white rectangles on merged images. Arrows point to examples of vesicular puncta displaying fluorescence through all channels (nonspecific colocalization). Arrowheads mark examples of areas of the plasma membrane exhibiting an overlap of fluorescence through 488-nm and 561-nm channels but no autofluorescence (apparent specific colocalization of mNG-KRAS and EGF-Rh). Scale bars are 10 μm and 5 μm in full images and insets, respectively.

Recombinant overexpressed RAS fusion proteins have been detected in early, late, and recycling endosomes, including those containing EGFR and Grb2 (e.g., Jiang and Sorkin, 2002; Lu et al., 2009; Schmick et al., 2014). Likewise, RAS and receptor tyrosine kinases were copurified in the endosomal fraction by differential centrifugation (Howe et al., 2001; Pol et al., 1998), although whether EGFR and RAS are present in the same endosome is not possible to prove using this latter methodology. In contrast, in HeLa cells, which are a commonly used model system to study EGFR signaling and trafficking because they express physiological levels of EGFR, the endogenous mNG-tagged KRAS and NRAS, in common with HRAS (Pinilla-Macua et al., 2016), were found to be predominantly localized to the plasma membrane (Fig. 1), and their subcellular distribution did not change upon stimulation with EGF. Only a small pool of endogenous mNG-KRAS is detected in conventional vesicular endosomes. The previously reported localization of KRAS to mitochondria (Bivona and Philips, 2003; Bivona et al., 2006; Hu et al., 2012; Rebollo et al., 1999) was not observed when imaging endogenous KRAS. Similarly, no significant presence of endogenous NRAS in vesicular endosomes was observed, regardless of EGF stimulation, even though NRAS was commonly concentrated to the Golgi area. In this area, NRAS was partially colocalized with markers of trans-Golgi (GRASP55) and PRC (Rab11). Although precise localization of proteins in the “congested” Golgi area is difficult to define by confocal microscopy due to the high concentration of membrane compartments in this area, endogenous NRAS typically displayed significant overlap with GRASP55, a protein enriched in trans-Golgi/medial Golgi cisternae (Fig. 3). This differs from the relatively rare detection of overexpressed HA-tagged NRAS in the trans-cisterna within the Golgi complex by EM (Lynch et al., 2015).

3D imaging of endogenous mNG-NRAS led us to propose the existence of an uninterrupted tubular membrane network connecting the plasma membrane and the PRC, which we termed “TERC.” These diffraction-limited tubular shaped structures were seen as either plasma membrane protrusions or recycling tubules emanating from the Golgi area, but frequently as “tracts” linking the plasma membrane with the PRC. Morphologically similar compartments were observed in cells expressing endogenous mVenus-HRAS (Pinilla-Macua et al., 2016). Two lines of evidence support the plasma membrane origin of TERC (Fig. 4). First, the tubules were stained with the plasma membrane dye CellMask. Second, these tubular compartments contained PIP2, a phospholipid that is highly enriched in the plasma membrane. Tubular protrusions from the plasma membrane have previously been observed in cells overexpressing HRAS and implicated in clathrin-independent endocytosis (Day et al., 2015). Although endogenous mNG-NRAS was present in the TERC in ~20% of cells at any given time and the fraction of total

mNG-NRAS located in these compartments was relatively small, the amount of recombinant HRAS in tubular protrusions of the plasma membrane appeared to be much more substantial (Day et al., 2015). Importantly, we showed that the recycling Rab, Rab11a, and EHD1, an ATPase involved in endosomal recycling, are present in NRAS-containing TERCs that spun from the plasma membrane to the Golgi area, suggesting that they can be involved in cargo recycling and anterograde transport to the plasma membrane. In our previous study, endogenous HRAS was also seen in TERC labeled with Rab11 in the Golgi-proximal region and EHD1 in the Golgi-distal region of TERCs (Pinilla-Macua et al., 2016). Interestingly, enrichment in PIP2 was previously reported in tubular structures that were classified as recycling endosomes (Farmer et al., 2021). Thus, we hypothesize that the TERC network allows bidirectional diffusion-based transport of proteins and lipids between the plasma membrane and the Golgi area (PRC) as opposed to the conventional cargo traffic involving membrane carriers shuttling between donor and target membranes. Because trafficking of palmitoylated RAS isoforms was proposed to be mediated by recycling endosomes (Misaki et al., 2010), we further speculate that endorecycling nanotubes may be involved in the transport of post-translationally modified NRAS and HRAS to the plasma membrane. It is unclear whether a membrane fission-fusion event is involved in the communication between TERC and PRC in the juxta-Golgi area, although, given that both compartments are Rab11 labeled, the possibility of a continuous lateral membrane diffusion-based transport seems likely.

Based on live-cell imaging of endogenous components of the EGFR-ERK1/2 signaling pathway and an inhibitory analysis of this pathway, we propose a following working model of the spatiotemporal regulation of this signaling process in cells with low levels of EGFR expression. Grb2 is recruited from the cytosol and nucleus to cell surface EGFRs within 1–3 min of EGF stimulation. EGFR-Grb2 complexes are then rapidly internalized, resulting in their robust accumulation in endosomes observed after 3–5 min and sustained for at least 1 h. These observations are based on the first live-cell imaging analysis of endogenous fluorescent Grb2 (Fig. 7), although endogenous Grb2 and recombinant Grb2 have been shown to remain associated with internalized EGFR using immunofluorescence, live-cell microscopy, and subcellular fractionation in various cell types (Di Guglielmo et al., 1994; Fortian and Sorkin, 2014; Oksvold et al., 2000; Sorkin et al., 2000). Thus, EGFR-Grb2 complexes, some presumably associated with SOS, are transiently positioned in close proximity to RAS while passing through the plasma membrane during the initial 1–5 min after EGF stimulation, which correlates with the maximal activation of RAS in HeLa cells (Pinilla-Macua et al., 2016). Subsequent internalization of ~85–90% of EGFR-Grb2 complexes into early and sorting

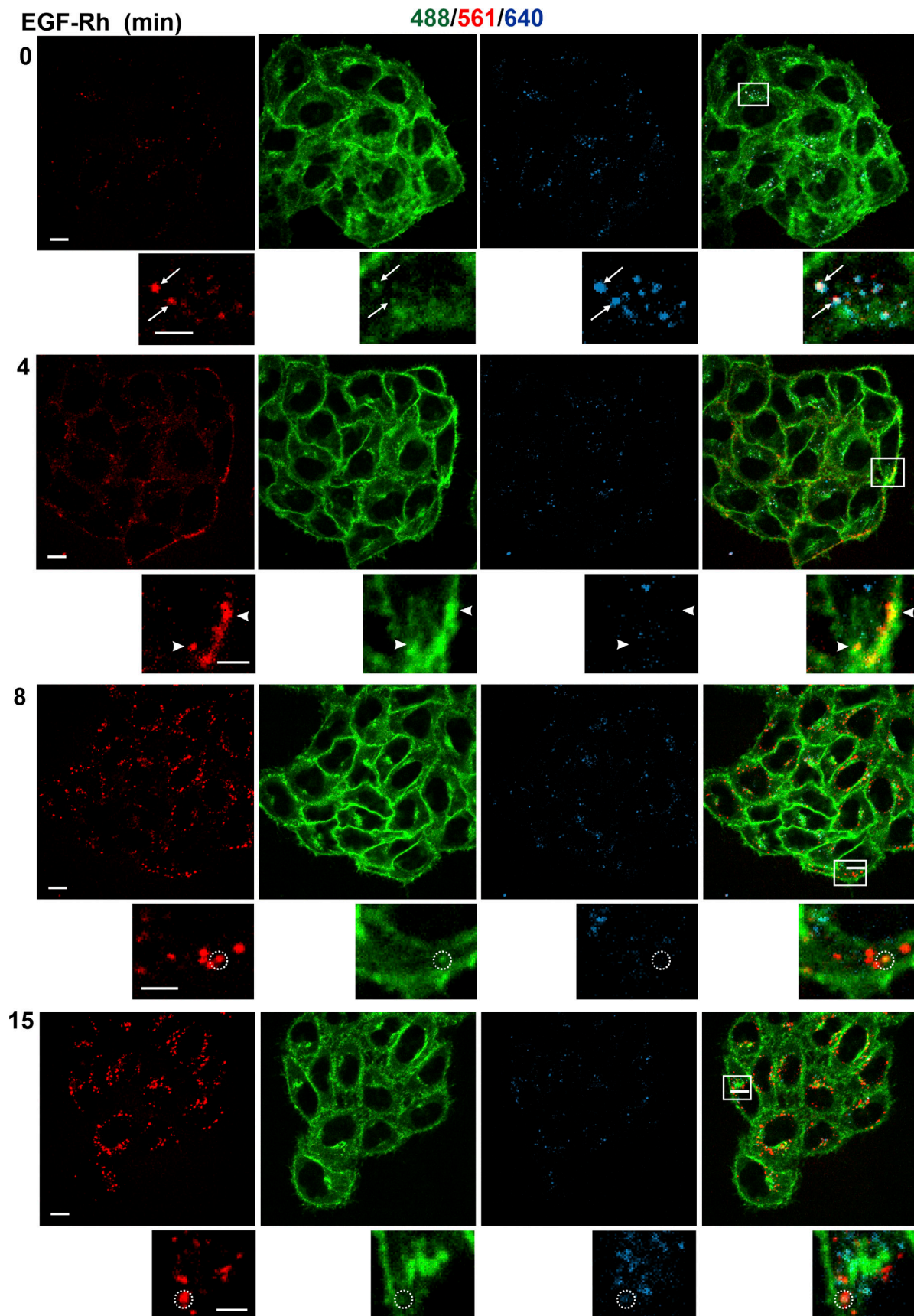


Figure 6. **Localization of mNG-NRAS in EGF-stimulated cells.** HeLa/mNG-NRAS cells were serum starved and treated with 4 ng/ml EGF-Rh at 37°C for the indicated times. 3D live-cell imaging was performed through 488-nm (green), 561-nm (red), and 640-nm (blue; autofluorescence) channels. Fluorescence

intensity scales are identical for full-size images at all time points. Individual confocal sections are shown. Insets are the high-magnification/contrast images corresponding to the regions indicated by white rectangles on merged images. Arrows point to examples of vesicular puncta displaying fluorescence through all channels (nonspecific colocalization). Arrowheads and white circles mark examples of, respectively, areas of the plasma membrane (4 min) and vesicular puncta (8 and 15 min) exhibiting an overlap of fluorescence through 488-nm and 561-nm channels but no autofluorescence (apparent specific colocalization of mNG-KRAS and EGF-Rh). Scale bars are 10 μm and 5 μm in full images and insets, respectively.

endosomes results in rapid (within 10 min) segregation of these complexes from all RAS species, which remain mainly localized at the plasma membrane, and from NRAS and HRAS, which are also present in PRC, Golgi, and TERC. Such segregation correlates with the decrease in RAS activity that plateaus at a low level (10–20% of maximum activity) after 10–15 min of EGF stimulation (Pinilla-Macua et al., 2016). It should be noted that we have not observed EGF-Rh in TERCs, probably because diffusion of a large transmembrane cargo, such as ligand-EGFR dimers, from the plasma membrane into thin tubules of TERCs is inefficient.

Although EGF-induced Grb2 recruitment to the receptor and maximal RAS activity at 3–5 min after EGF stimulation correlates with the onset of ERK1/2 activation, how the sustained activity of ERK1/2 is maintained beyond 10–15 min of EGF stimulation for the next 45–50 min and further remains unclear. Our previous study demonstrated that sustained activity of ERK1/2 requires EGFR kinase activity even after physical separation of HRAS from active EGFR (Pinilla-Macua et al., 2016). One possibility is that a small amount of RAS is present in vesicular endosomes containing EGFR-Grb2-SOS complexes, but that this pool is beneath the sensitivity of confocal imaging. Indeed, because of the substantial autofluorescence of vesicular endosomes, the sensitivity of detection of endogenous fluorescently tagged proteins in endosomes is somewhat limited. Although our spectral unmixing approach can be reliably used to measure the specific localization of adaptors such as Grb2 in endosomes, it is impossible to formally rule out that several molecules of RAS are present in each EGFR-containing endosome. At the same time, our previous studies of the dynamics of endogenous RAF1 trafficking, which can be considered as an endogenous sensor of GTP-loaded RAS, failed to detect significant amounts of GTP-loaded RAS in EGFR-containing endosomes, even in the presence of sorafenib, which stabilizes RAF at the membrane, and it was estimated that the presence of more than three molecules of labeled RAF1 per endosome would have been detected (Surve et al., 2019). It should also be noted that we have not been able to detect EGF-induced activation of endogenous mNG-tagged RAS using a variety of published fluorescent GTP-Ras sensors (Misaki et al., 2010; Wiechmann et al., 2020). This motivated us to generate double-edited cells, which allowed us to demonstrate that an endogenous sensor of GTP-RAS, mCh-tagged RAF1, was translocated to the plasma membrane and that TERC was labeled with mNG-NRAS in the presence of EGF and sorafenib (Figs. 9 and S4). Interestingly, RAF1-mCh was detected throughout the TERC, including in regions adjacent to or continuous with the PRC in cells stimulated with EGF in the presence of sorafenib for 1 h or longer, indicating the potential sustained activity of GTP-RAS deep inside the cell (Fig. 9). We speculate that RAS is initially activated by the EGFR-Grb2-SOS complex at the peripheral plasma membrane and then can

gradually diffuse into the TERC and reach the PRC. Alternatively, recruitment of RAF1-mCh may be due to local activation of RAS in the PRC. The Golgi area was previously reported to be the site of RAS activation via Grb2/SOS-independent mechanisms at late times after cell stimulation (Chiu et al., 2002). Altogether, our studies of the localization of endogenous HRAS, KRAS, NRAS, and RAF1 (Pinilla-Macua et al., 2016; Surve et al., 2019; and the present study) suggest that in the HeLa cell experimental system, even if RAS activation takes place in EGFR-containing endosomes, the contribution of this endosomal signaling to the overall EGF-induced activation of downstream kinases is expected to be extremely small.

A second possibility is that the sustained signaling to ERK1/2 is caused by a small pool of ligand-bound EGFR remaining in the plasma membrane, which is estimated to be $\sim 2,000$ – $3,000$ receptors per cell after 15 min of ligand stimulation (Fig. S3, B and C). The presence of active EGFRs at the cell surface after 15 min of EGF stimulation, although not readily measurable by confocal microscopy, is supported by detection of EGFR using cell surface biotinylation (Pinilla-Macua et al., 2016) and by the sustained presence of increased levels of Grb2 on the basal cell membrane detected by TIRF microscopy (Fig. 7). Most important, in the present study, the observation that blocking cell surface EGFR by cetuximab after 15 min of EGF-stimulated endocytosis caused dramatic down-regulation of MEK1/2 and ERK1/2 activities (Fig. 8, C–E) provides crucial functional evidence for the role of a noninternalized pool of ligand-bound EGFRs in maintaining signaling through the RAS-RAF-MEK-ERK axis from the plasma membrane. Cumulatively, demonstration of the prominent plasma membrane localization of endogenous tagged KRAS, NRAS and HRAS by live-cell imaging, detection of a small but sustained active (Grb2-bound) EGFR pool at the cell surface and the effect of cetuximab suggest that cell-surface EGFRs persistently contribute to signaling along the EGFR-RAS-ERK1/2 pathway.

If the plasma membrane is the site of initiation and maintenance of RAS-ERK signaling and only a few active EGFRs are sufficient to maintain the signaling, EGFR endocytosis is unlikely to play a significant role in the signaling mechanism. This is reinforced by the inhibition of clathrin-mediated endocytosis using two independent approaches, which did not significantly affect the time course of EGF-induced ERK1/2 activity (Fig. 8) and which confirmed that EGFR endocytosis is not an essential process for EGF-induced ERK1/2 activation in HeLa cells. Furthermore, reduced endocytosis did not result in a significant increase of the ERK1/2 activity after 20 min or longer of EGF stimulation, even though a considerable pool of EGFR remained at the plasma membrane in the absence of efficient endocytosis (Fig. S3). It is likely that other mechanisms of negative feedback regulatory signaling control the amplitude and kinetics of the pathway activation downstream of RAS when endocytosis is

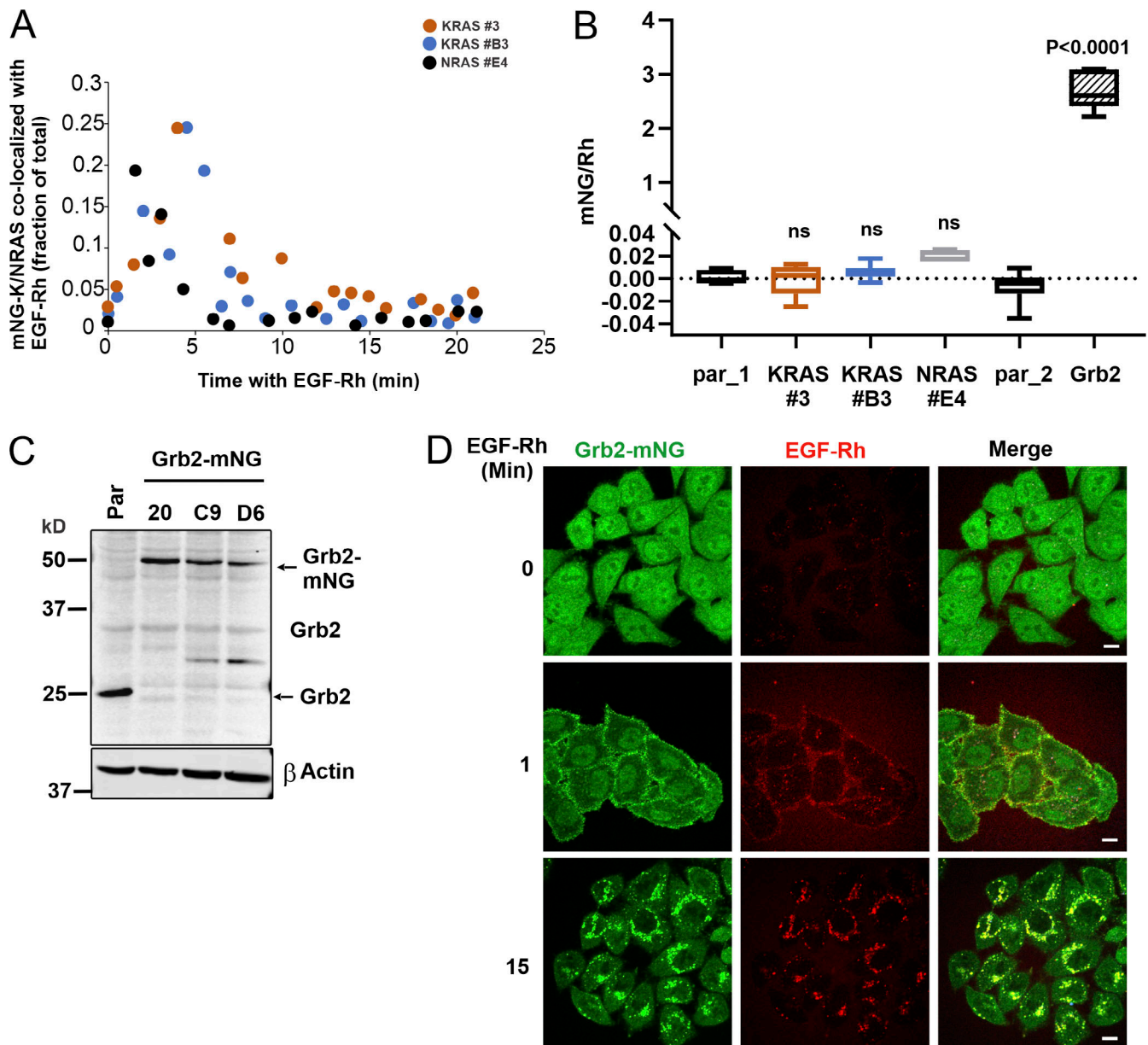


Figure 7. Quantification of colocalization of mNG-KRAS, mNG-NRAS, and Grb2-mNG with EGF-Rh. (A) The fractions of total mNG-KRAS (two single-cell clones) and mNG-NRAS (one clone) colocalized with EGF-Rh were calculated from time course imaging experiments presented in Figs. 5 and 6 and as described in Materials and methods. (B) Quantifications of the background fluorescence through the 640-nm channel, specific fluorescence intensities of mNG and Rh through 488- and 561-nm channels, and the ratio of these specific fluorescence intensities (mNG/Rh) in vesicular compartments were performed in 3D images from time course experiments (5–20-min incubation with EGF-Rh) exemplified in Figs. 5 and 6, as described in Materials and methods. Medians and ranges (minimum and maximum values) are shown on box plots. P values for mNG-RAS-expressing clones against parental cells (par_1) were calculated using multiple comparison ANOVA. The P value for Grb2-mNG against parental cells (par_2) was calculated using Student's *t* test. (C) Lysates from parental (Par) HeLa cells and several Grb2-mNG gene-edited clones were probed with Grb2 and β -actin (loading control) antibodies. All clones were homozygous. (D) HeLa/Grb2-mNG cells were serum starved and treated with 4 ng/ml of EGF-Rh at 37°C for the indicated times. 3D live-cell imaging was performed through 488-nm (green; mNG), 561-nm (red; EGF-Rh), and 640-nm (blue; autofluorescence; not shown) channels. Single confocal sections are shown. Scale bars, 10 μ m. The images from 5–20-min time points were used to calculate specific 488-nm fluorescence and the mNG/Rh ratio in B. Parental cells were imaged using the same imaging parameters used for Grb2-mNG cells for calculations presented in B.

attenuated (Buday et al., 1995; Lake et al., 2016). To conclude, it is important to consider that a “negative” function of endocytosis (i.e., separation of EGFR–Grb2 complexes from the major pool of RAS) may not be universally applicable to all cell types. This is clearly illustrated by contrasting effects of endocytosis inhibitors on this signaling pathway in different experimental cell

models (DeGraff et al., 1999; Galperin and Sorkin, 2008; Johannessen et al., 2000; Roy et al., 2002; Sousa et al., 2012; Teis et al., 2002; Vieira et al., 1996; Whistler and von Zastrow, 1999). Future studies of the localization dynamics of endogenous RAS and RAF in cells of a different origin and with different EGFR expression levels may uncover important variabilities in the contribution

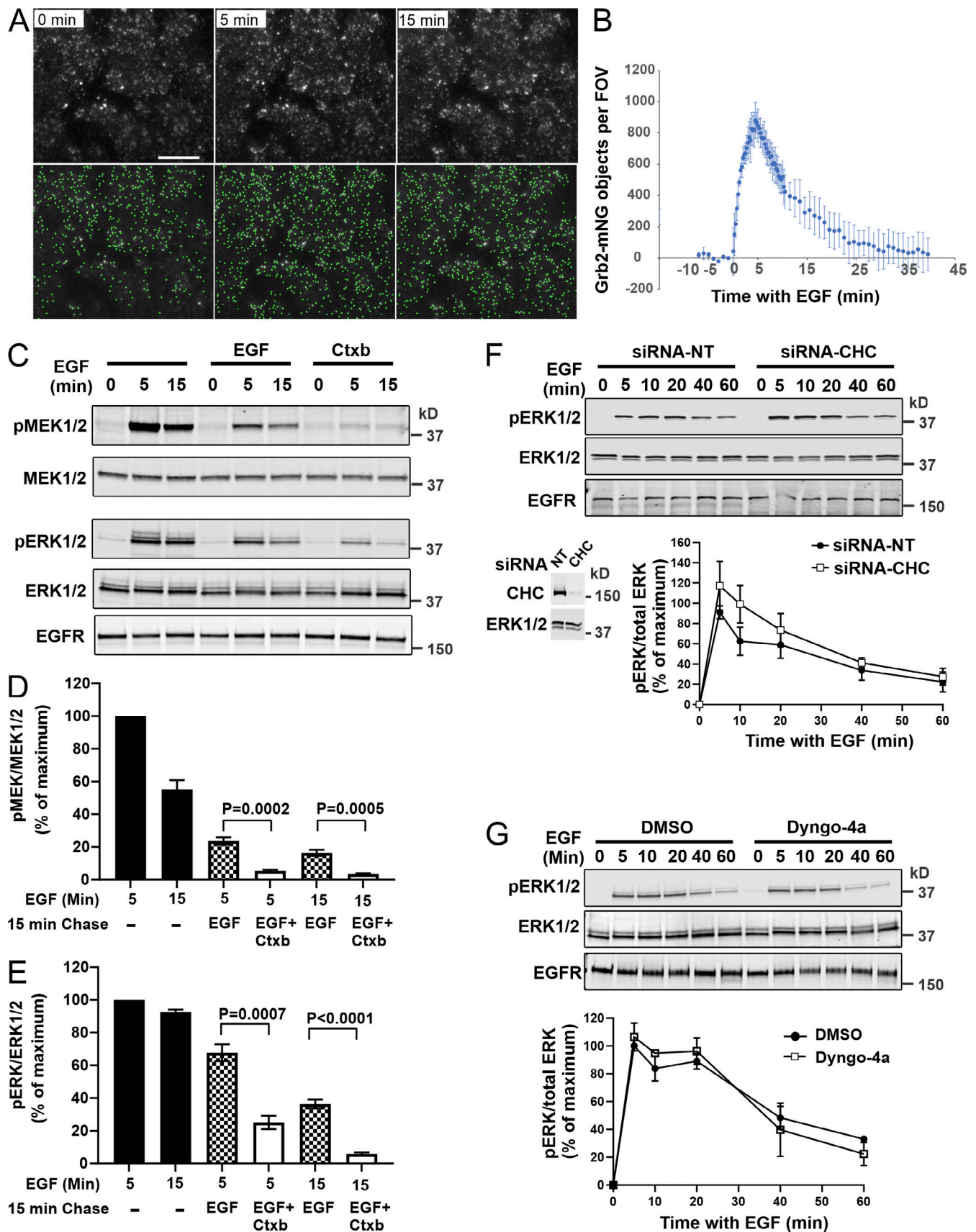


Figure 8. Sustained signaling from EGFR to ERK1/2 is dependent on the activity of the cell surface pool of EGFR and unaffected by the inhibition of endocytosis. (A) Serum-starved HeLa/Grb2-mNG cells were imaged by TIRF microscopy before and after stimulation with EGF (4 ng/ml) at 37°C. Selected time

frames before EGF addition and after 5 min and 15 min of cell incubation with EGF are shown in the top row. Corresponding images of individual objects defined as the diffraction-limited puncta are shown in the bottom row. **(B)** Quantification of the number of Grb2-mNG puncta per FOV in time course sequences exemplified in A was performed as described in Materials and methods. Mean object numbers per FOV from the last six time points before EGF stimulation were calculated (EGF-independent background) and subtracted from the object numbers quantitated at each time point after EGF stimulation in corresponding FOVs. Mean values of background-subtracted object numbers per FOV ($n = 3$) with SDs are plotted against time. **(C)** Effect of EGFR inhibition by cetuximab (Ctxb). Serum-starved parental HeLa cells were stimulated with 1 ng/ml EGF for 5 or 15 min. The cells were either lysed or further incubated with EGF and with or without cetuximab (5 $\mu\text{g/ml}$) for an additional 15 min (15 min chase). Lysates were subjected to Western blotting with pMEK1/2, total MEK1/2, pERK1/2, total ERK1/2, and EGFR antibodies. **(D and E)** MEK1/2 (D) and ERK1/2 (E) activities were quantitated from experiments exemplified in C and expressed as the percentage of the maximum activity after 5 min of EGF stimulation. Bar graphs represent mean values (\pm SEM) obtained from four independent experiments. P values against cetuximab-untreated cells were calculated using an unpaired Student's *t* test. **(F)** Parental HeLa cells were transfected with nontargeting (NT) or CHC targeted siRNAs. 3 d after transfection, the cells were stimulated with EGF (4 ng/ml) for the indicated times at 37°C. The lysates were probed by Western blotting with pERK1/2, CHC, ERK1/2, and EGFR antibodies. ERK1/2 activity was measured as described in E and expressed as the percentage of the maximum activity in NT-transfected cells. Mean values with SEMs ($n = 3$) are plotted against time. **(G)** Parental HeLa cells were pretreated with vehicle (DMSO) or Dyngo-4a (30 μM) for 30 min at 37°C and then stimulated with EGF (4 ng/ml) for the indicated times at 37°C. The aliquots of lysates were probed by Western blotting with pERK1/2, total ERK1/2, and EGFR antibodies. ERK1/2 activity was measured as described in E and expressed as the percentage of the maximum activity in vehicle-treated cells. Mean values with SEMs ($n = 3$) are plotted against time.

of endocytosis and endosomal signaling in the spatiotemporal regulation of the EGFR-RAS-ERK1/2 signaling pathway.

Materials and methods

Reagents

Recombinant human EGF was purchased from BD Biosciences. EGF-Rh was purchased from Molecular Probes. Mouse mAb to MEK1/2 (catalog no. 4694) and phosphorylated ERK1/2 (catalog no. 9106), rabbit mAb to phosphorylated MEK1/2 (catalog no. 2338) and rabbit polyclonal to ERK1/2 (catalog no. 9102), rabbit polyclonal antibody to α -actinin (catalog no. 3134), and rabbit mAb to GAPDH (catalog no. 2118) were from Cell Signaling Technology. Mouse mAb to NRAS (sc-31), rabbit polyclonal antibody to Grb2 (sc-255), mouse mAb to GAPDH (sc-47724), and mouse mAb to β -actin (sc-8432) were from Santa Cruz Biotechnology. KRAS recombinant rabbit mAb (703345) was purchased from Thermo Fisher Scientific. Secondary antimouse (catalog nos. 926-32220, 926-32210, and 926-32350) and anti-rabbit (catalog nos. 926-32211 and 926-68071) IRDye antibodies were from LI-COR. Mouse mAbs to EEA1 (E41120) and RAF1 (R19120) were from BD Transduction Laboratories. Goat antihuman secondary antibody conjugated to Alexa Fluor 488 (109-545-098) was from Jackson ImmunoResearch. Cetuximab (humanized mouse mAb to EGFR) was purchased from Sigma-Aldrich (MSQC18) and MedChemExpress (HY-P9905). Rabbit polyclonal antibody to CHC (ab21679) was purchased from Abcam. Dyngo-4a was from Abcam. All oligonucleotides listed in Table 1 were purchased from Integrated DNA Technologies (IDT). CHC siRNA duplexes were purchased from Dharmacon. Sorafenib was purchased from Santa Cruz Biotechnology and stored as 10 mM stock solution in DMSO at -20°C . CellMask Deep Red Plasma Membrane Stain (CellMask) and Lipofectamine transfection reagents were from Thermo Fisher, whereas jetOptimus transfection reagent was purchased from Polyplus. PCR and cloning reagents were purchased from New England Biolabs (NEB).

CRISPR/Cas9 gene editing of HeLa cells to tag proteins with mNG

To generate cells expressing mNG-KRAS and mNG-NRAS, gRNAs were synthesized using the GeneArt precision gRNA

synthesis kit (Invitrogen) according to the manufacturer's instructions. gRNA sequences were selected using online algorithms to target regions of *KRAS* and *NRAS* genes situated close to start codons. Forward and reverse single-stranded oligonucleotides were ordered from IDT (Table 1) to generate a DNA assembly for gRNA by a short PCR that incorporated T7 promoter and the constant region of trans-activating CRISPR RNA. Using this DNA assembly, in vitro transcription reactions with nucleoside triphosphate mix and T7 RNA polymerase were performed at 37°C for 2 h, followed by treatment with DNase I for 15 min at 37°C to remove contaminating DNA. Finally, gRNAs were purified using a column provided in the kit. Appropriate precautions throughout the procedure were taken to avoid RNase contamination in the final gRNA product. Synthetic double-stranded donor DNAs, consisting of the mNG sequence flanked by \sim 500 bp of 5' and 3' homology arms, were obtained from IDT. Donor DNAs were amplified and cloned into a pCR-BluntII-TOPO plasmid (Invitrogen). The inserts (1.7 kb) were prepared by EcoRI digestions for transfections. The first round of transfection was performed using a Neon electroporation system (Invitrogen). RNP complex was generated in Buffer R by incubating 1 μg of Platinum Cas9 (Invitrogen) and 0.5 μg of in vitro transcribed gRNA at RT for 20 min. 5×10^5 HeLa cells and double-stranded donor were added to the RNP complex just before the electroporation. The total volume of the mix was adjusted to 10 μl , and the cells were electroporated at 1,005 V in two pulses of a 35-ms pulse width. The cells were then allowed to recover and expand. Cells positive for mNG were sorted using a BD FACSAria III sorter (BD Biosciences) and underwent the second round of transfection using Lipofectamine CRISPRMAX Cas9 transfection reagent (Invitrogen). To this end, a mixture of 0.5 μg gRNA and 1 μg purified Cas9 and Cas9-plus reagent was incubated at RT for 10 min in OptiMEM (Invitrogen) to allow the formation of the RNP complex, followed by the addition of 1 μg donor insert. 3 μl of CRISPRMAX reagent was mixed with the RNP complex, incubated for 10 min at RT, and added dropwise to cells in a well of a 12-well plate in 1 ml DMEM (Invitrogen). Similar to the first round of transfection, mNG-positive cells were sorted using flow cytometry into 96-well plates to select single-cell clones. The expression of mNG-fusion proteins was validated

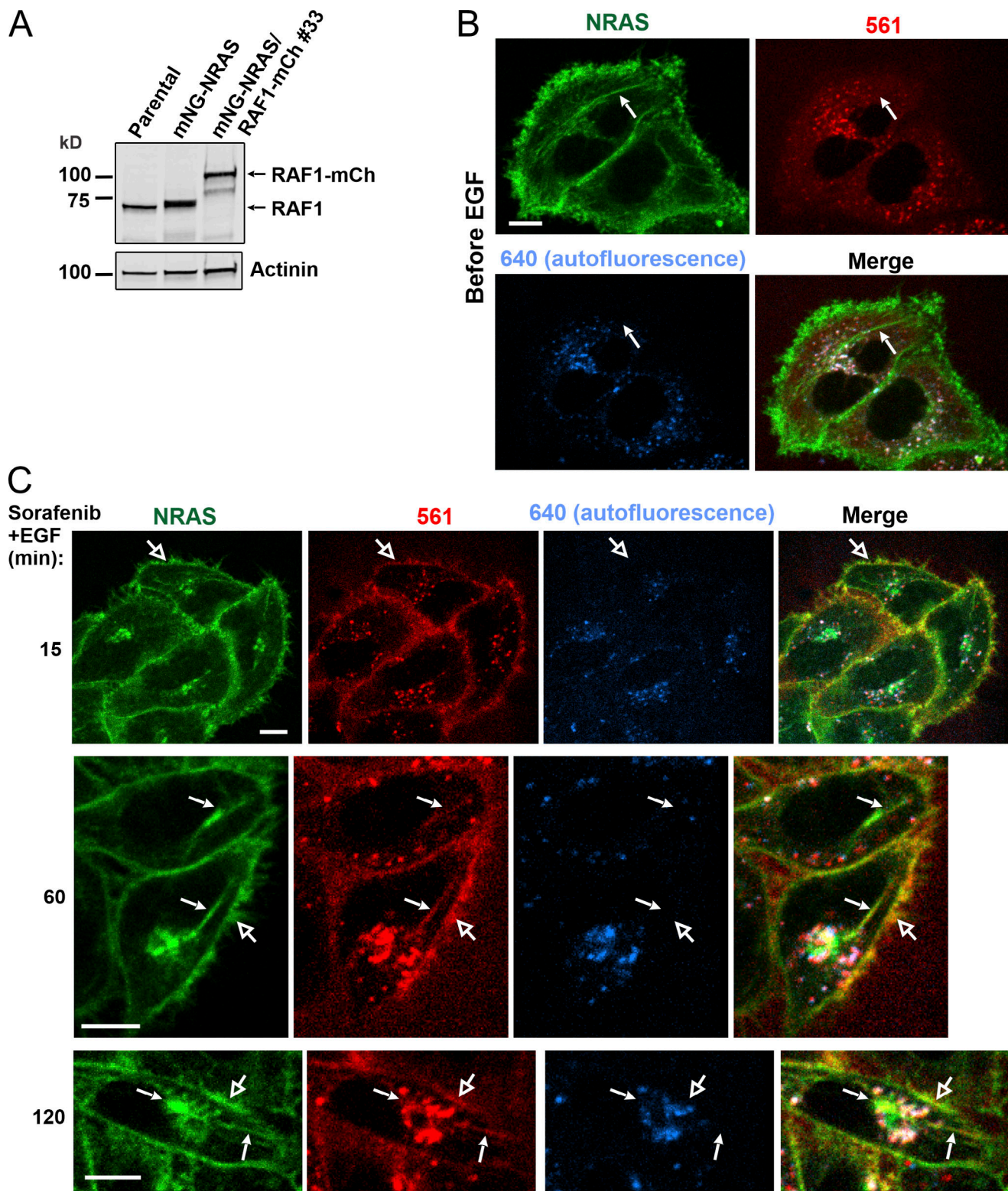


Figure 9. **Recruitment of endogenous RAF1-mCh- to mNG-NRAS-labeled plasma membrane, TERC, and PRC in double-gene-edited cells.** (A) Cell lysates from parental HeLa, HeLa/mNG-NRAS, and HeLa/mNG-NRAS/RAF1-mCh cells were probed by Western blotting with RAF1 and α -actinin (loading control) antibodies. (B and C) Live HeLa/mNG-NRAS/RAF1-mCh cells were imaged at 37°C before (B) and after (C) stimulation with 4 ng/ml EGF and sorafenib (10 μ M) through 488-nm (green; mNG), 561-nm (red; mCh), and 640-nm (blue; autofluorescence) channels. Maximum-intensity z-projections of two consecutive confocal images are shown. Filled arrows point to examples of colocalization of RAF1-mCh and mNG-NRAS in endorecycling nanotubules and the PRC. Open arrows indicate the plasma membrane colocalization of mNG-NRAS and RAF1-mCh. Strong vesicular 561-nm channel fluorescence represented autofluorescence as evident by colocalization of vesicles with the puncta detected through the 640-nm channel. Scale bars, 10 μ m.

Table 1. gRNAs, sequencing primers, and siRNA

Primer	Sequence 5'-3'	Purpose
Kras_1F	5'-TAATACGACTCACTATAGGAATATAAACTTGTGGTAGT-3'	Generation of KRAS and NRAS gRNAs
Kras_1R	5'-TTCTAGCTCTAAACACTACCACAAGTTTATATTC-3'	
Kras_2F	5'-TAATACGACTCACTATAGAATGACTGAATATAAACTTG-3'	
Kras_2R	5'-TTCTAGCTCTAAACCAAGTTTATATTCAGTCATT-3'	
Nras_1F	5'-TAATACGACTCACTATAGGACTGAGTACAACTGGTGG-3'	
Nras_1R	5'-TTCTAGCTCTAAACCCACCAGTTTGTACTCAGTC-3'	
Nras_2F	5'-TAATACGACTCACTATAGAATGACTGAGTACAACTGG-3'	Sequencing of KRAS and NRAS clones
Nras_2R	5'-TTCTAGCTCTAAACCCAGTTTGTACTCAGTCATT-3'	
KrasutrF1	5'-GCGTCGATGGAGGAGTTTG-3'	
KrasR2	5'-ACTCTTGCTACGCCACCA-3'	
NrasutrF1	5'-GGGGAGATCTTTGGAGACAGAA-3'	
NrasR2	5'-TGGGTAAAGATGATCCGACAAGT-3'	
grb2-RNA_T1	5'-ATCTTGTGAAAGGACGAAACACCGGGTTAGACGTTCCGGTTCACGGGTTTTAGAGCTAGAAATAGCA AGTT-3'	Generation of Grb2 gRNAs
grb2-gRNA_T2	5'-ATCTTGTGAAAGGACG AAACACCGGGCTTAGACGTTCCGGTTCACGGGTTTTAGAGCTAGAAATAGCA AGTT-3'	
Grb-HA_f	5'-TATCGATAAGCTTGATATCGAGAGGAGGTGTAGCCAG-3'	Generation of Grb2-mNG donor
Grb-HA_r	5'-CTCCTCCTAAGACGTTCCGGTTCACGGG-3'	
Grb-Neon_f	5'-CCGGAACGTCTTAGGAGGAGGAGGATCAG-3'	
Grb-Neon_r	5'-TTGACTCTTACTTGTACAGCTCGTCCATG-3'	
Grb-3HA_f	5'-GCTGTACAAGTAAGAGTCAAGAAGCAATTATTTAAAG-3'	
Grb-3HA_r	5'-CCACCGCGGTGGCGGCCGCTTCTCGAACTCTGACCTTG-3'	
mCh-F3	5'-ATGGTGAGCAAGGGCGAG-3'	Generation of RAF1-mCh donor
mCh-R2	5'-CTTGTACAGCTCGTCCATGC-3'	
mCh_F4	5'-CTTGACGCTGACCCAGCTCCCGAGGCTGCCTGTCTTCTTAGGAGGA-3'	
	5'-GGAGGATCAGCAGCAGCAATGGTGAGCAAGGGCGAG-3'	
mCh_R3	5'-CTGAAGACAGGTGCAAAGTCAACTACTTGTACAGCTCGTCCATG-3'	
CHC siRNA	5'-GCAATGAGCTGTTTGAAGA-3'	CHC knockdown

Underlined sequences correspond to target gRNA sequence.

by Western blotting and DNA sequencing to ensure correct insertion of mNG.

To insert mNG at the C-terminus of Grb2 protein, two gRNA target sequences were identified close to the stop codon of *GRB2* using online algorithms. The target sequence was cloned in pSpCas9(BB)-2A-Puro (PX459) plasmid (gift from Feng Zhang, Broad Institute, Cambridge, MA; Addgene plasmid 62988; [Ran et al., 2013](#)) using the NEBuilder HiFi DNA Assembly kit (NEB). PX459 plasmid was digested with BbsI. 0.2 μM single-stranded DNA oligonucleotide (grb2-gRNA_T1 and grb2-gRNA_T2; [Table 1](#)), and 50 ng of linearized PX459 were ligated using HiFi DNA Assembly mix. DH5α *Escherichia coli*-competent cells were transformed with 2 μl of the ligation mixture. Positive colonies containing gRNA were confirmed by restriction enzyme digestion and sequencing. To clone donor DNA for Grb2 gene editing, 5' and 3' homology arms were amplified from HeLa genomic DNA using primers designed by the NEbuilder algorithm (NEB),

whereas KRAS donor DNA was used as a template to amplify mNG ORF ([Table 1](#)). The PCR amplicons were gel eluted. EasyFusion Halo plasmid (a gift from Janet Rossant, The Hospital for Sick Children, Toronto, Canada; Addgene plasmid 112850) was digested with EcoRI and XbaI to remove the Halo insert. Linear EasyFusion Halo plasmid was used as a backbone for cloning 5' HA, mNG, and 3' HA in a HiFi DNA assembly ligation reaction. The ligation mixture was used to transform DH5α *E. coli*-competent cells. Positive colonies were confirmed by digestion and sequencing. The resulting plasmid is denoted as the "Grb2-mNG donor." HeLa cells were transfected with PX459 plasmid containing gRNAs and Grb2-mNG donor using Lipofectamine 3000 at a ratio of 1:3, respectively, and grown with puromycin (2 μg/ml) for 2 d to enrich for transfected cells. The cells were then diluted to allow single-cell colony isolation and plated in a 10-cm dish. Colony screening was performed by Western blotting using the Grb2 antibody.

To generate double gene-edited HeLa/RAF1-mCh/mNG-NRAS cells, mCh fragment was amplified from plasmids coding for mCh-Rab11 using primers mCh_F3 and mCh_R2 (Table 1). The linker sequence and overlapping sequence were added to the mCh fragment using primers mCh_F4 and mCh_R2. This second mCh fragment was used for HiFi DNA assembly. The backbone vector for HiFi DNA assembly was generated by digestion of pUC18-RAF1 donor (Surve et al., 2019) with *Ava*I and *Hinc*II restriction enzyme digestion. mCh fragment was cloned in the backbone vector using HiFi DNA Assembly mix. HeLa/mNG-NRAS cells were transfected with a PX459 plasmid expressing RAF1 gRNA 3 (Surve et al., 2019) and RAF1-mCh donor plasmid using jetOptimus transfection reagent at a ratio of 1:3. The cells were diluted for single-cell clonal selection and plated onto a 10-cm plate. The colonies were screened using fluorescence microscopic imaging and Western blotting with the RAF1 antibody.

Cell culture and transfections

HeLa cells were grown in DMEM with 10% FBS (Invitrogen). The identity of HeLa cells was confirmed by short tandem repeat profiling. The cells were also tested for mycoplasma contamination using the MycoAlert kit (Lonza).

Parental and gene-edited HeLa cells were transiently transfected with 0.3–0.5 μ g of DNA plasmids using Lipofectamine 3000 (Invitrogen) in a 12-well plate. The constructs used were as follows: mRFP-APPL1 (a gift from Pietro De Camilli, Yale University School of Medicine, New Haven, CT; Addgene plasmid 22202), mRFP-Rab5 (Galperin et al., 2004), CFP-Rab7 (Galperin and Sorkin, 2008), mCh-Rab11a (provided by Dr. Ora Weisz, University of Pittsburgh, Pittsburgh, PA), Tomato-EHD1 (provided by Dr. Steve Caplan, University of Nebraska, Omaha, NE), GRASP55-mCh (provided by Dr. Adam Linstedt, Carnegie Mellon University, Pittsburgh, PA), and pmCH-PH-PLC δ 1 (provided by Dr. Gerry Hammond, University of Pittsburgh, Pittsburgh, PA). The transfected cells were plated into 35-mm MatTek dishes (MatTek Corporation) 1 d after transfection and used for live-cell imaging after 48–72 h.

For RNAi experiments, HeLa parental cells were grown in 35-mm plates to ~70% confluency. The cells were either transfected with 20 μ M nontargeting control siRNA or CHC-specific siRNA (Huang et al., 2004) using DharmaFect transfection reagent. On the next day, the transfected cells were replated into six-well plates and used for experiments 2 d after transfection.

Spinning-disk confocal microscopy

For live-cell 3D imaging, cells were grown in MatTek dishes. We used a spinning-disk confocal Marianas system based on the Zeiss Axio Observer Z1 inverted fluorescence microscope and CSU-W1 spinning disk, equipped with 405-, 445-, 488-, 515-, 561-, and 640-nm lasers, 63 \times /1.4 NA oil immersion objective, an Evolve electron-multiplying charge-coupled device camera, and piezo-controlled z-step motor, all controlled by SlideBook 6 software (Intelligent Imaging Innovation). The system was also equipped with an environmental chamber to maintain 37°C and 5% CO₂. Typically, a z-stack of 15 x–y confocal images was acquired at 0.2–0.4- μ m steps. SlideBook 6 was used for image analysis.

Measurement of the plasma membrane fractions of mNG-NRAS and mNG-KRAS

To quantify the amount of mNG-KRAS and mNG-NRAS located in the plasma membrane, CellMask was added to cell media at RT or 4°C, and cells in 35-mm MatTek dishes were placed on the microscope stage for imaging at RT through 640-nm (CellMask) and 488-nm (mNG) channels. Ice was placed on top of dishes with 4°C medium during imaging. 3D images were deconvolved using a No Neighbors algorithm of SlideBook 6. A segment mask was generated from background-subtracted images to select all voxels detected through the 640-nm channel (Mask-640). Another segment mask was generated with the minimum threshold to include voxels detected through the 488-nm channel (total mNG-RAS). For both masks, identical threshold parameters were used for experimental variables. A “colocalization” mask was then generated to select voxels overlapping in Mask-640 and mNG-RAS masks. The sum fluorescence intensity of the 488-nm channel in the colocalization mask was divided by the sum fluorescence intensity of the mNG-RAS in each field of view (FOV) to calculate the fraction of total cellular mNG-RAS colocalized with CellMask.

Measurement of the fraction of mNG-RAS colocalized with EGF-Rh

To quantify the amount of mNG-KRAS and mNG-NRAS colocalized with EGF-Rh, 3D images of cells stimulated with EGF-Rh were deconvolved using a No Neighbors algorithm of SlideBook 6. A segment mask was generated from background-subtracted images to select voxels detected through the 561-nm channel (Mask-561). Another segment mask was generated with the minimum threshold to include all voxels detected through the 488-nm channel (total mNG-RAS). For both masks, identical threshold parameters were used for experimental variables. A “colocalization” mask was then generated to select voxels overlapping in Mask-561 and mNG-RAS masks. The sum fluorescence intensity of the 488-nm channel in the colocalization mask was divided by the sum fluorescence intensity of the mNG-RAS in each FOV to calculate the fraction of total cellular mNG-RAS colocalized with EGF-Rh.

Measurement of the ratio of fluorescence intensities of mNG and EGF-Rh in endosomes

The ratio of EGF-Rh and mNG-labeled proteins in endosomes was calculated using spectral unmixing as described previously (Surve et al., 2019). Parental HeLa, HeLa/mNG-KRAS, HeLa/mNG-NRAS, and HeLa/Grb2-mNG cells grown in MatTek dishes were placed on the microscope stage, and 3D images were acquired before and after cell stimulation with EGF-Rh at 37°C through 488-nm, 561-nm, and 640-nm channels for 20–25 min. The image acquisition parameters were kept constant for all variants in the same experiment.

To analyze images of mNG-N/KRAS-expressing cells, a segment mask 1 was created to select vesicles positive for 561-nm fluorescence using a low-intensity threshold of 4,000 arbitrary linear units of fluorescence intensity (a.l.u.f.i.). Objects smaller than 4 voxels were eliminated from this mask. In cells incubated with EGF-Rh for >10 min, mask 1 predominantly selects vesicles

containing EGF-Rh-EGFR complexes as well as autofluorescent vesicles in parental cells. Mask 2 was generated by dilation of individual objects in mask 1 by two voxels in three dimensions to measure background for mask 1 objects. Another segment, mask 3, was created to select voxels with 488-nm channel fluorescence using a low-intensity threshold of 4,000 a.l.u.f.i. Objects <200 voxels were eliminated in this mask. This mask predominantly selects plasma membrane mNG-KRAS/mNG-NRAS (which is often a single object or several continuous objects in each cell) and mNG-NRAS in the Golgi area. Mask 3 does not include EGF-Rh-containing vesicles, because the intensity of 488-nm channel fluorescence in these vesicles is <4,000 a.l.u.f.i. Next, “561endo” and “Dil-561endo” masks were generated by subtracting mask 3 from mask 1 and mask 2, respectively, to eliminate voxels overlapping with the plasma membrane and bright Golgi area fluorescence. Mask 561endo was subtracted from Dil-561endo mask to generate the background mask (Back-561endo). Finally, mean intensities of the Back-561endo mask in each channel were subtracted from mean intensities of the same channels in the 561endo mask to calculate mean background-subtracted intensities (I488, I561, and I640) of each channel per a FOV depicting multiple cells.

Mean values of the ratio of “488/640” were first calculated from multiple FOVs in parental cells to obtain the autofluorescence correction coefficient (k_{auto}). Mean values of k_{auto} were 1.36 and 1.32 in two independent experiments. k_{auto} was used to calculate the autofluorescence component (I488_{auto}) of the I488-channel fluorescence measured in mNG-KRAS/mNG-NRAS-expressing cells in each FOV using the equation $I488_{\text{auto}} = k_{\text{auto}} \times I640$. I488_{auto} was then subtracted from I488 to obtain a mean specific fluorescence intensity of mNG. I561 channel fluorescence in endosomes of cells incubated with EGF-Rh for ≥ 10 min was considered to be the specific Rh fluorescence. The mNG/Rh ratio in endosomes was calculated as the ratio of mean intensities of mNG and I561 per FOV.

The mean values of the mNG/Rh ratio were calculated in HeLa/Grb2-mNG cells stimulated with EGF-Rh as described above for calculations in mNG-KRAS/mNG-NRAS images, except that mask 3 was not generated, because high intensity of Grb2-mNG fluorescence in endosomes compared with that in the cytoplasm eliminated the need for excluding nonendosomal objects from mask 1 and mask 2. Mask 1 was directly subtracted from Mask 2 to generate the background mask (Back-561endo). Mean intensities of Back-561endo mask in each channel were subtracted from mean intensities of the same channels in mask 1 to calculate mean background-subtracted intensities in each channel (I488, I561, and I640) per a FOV depicting multiple cells.

TIRF microscopy

Time lapse TIRF microscopic imaging of serum-starved HeLa/Grb2-mNG cells was performed in 35-mm MatTek dishes before and during EGF stimulation using a Nikon Eclipse Ti inverted microscope (Nikon), a 100 \times /1.49 NA oil-immersion objective, a Photometrics 95B camera, an ILAS2 ring TIRF illuminator (Gataca Systems), and an Oxxius laser launch (Oxxius) through a 488-nm laser channel at 37°C and 5% CO₂ in starvation medium. Images were acquired every 60 s for 15 min before EGF

stimulation, every 30 s 10 min after EGF stimulation, and then every 60 s for 30 min. Image analysis was performed using Nikon Elements software. An intermediate 1.5 \times magnification changer was used to slightly oversample diffraction-limited spots (200 nm) with the 11- μ m pixel 95B camera. The diffraction-limited spot was therefore sampled at slightly over Nyquist frequency (at least 3 pixels/resolvable element). Diffraction-limited spots were defined by baseline intensity and size using the “spot” function in NIS-Elements; no downstream processing or enhancement of the raw datasets was performed. The total number of diffraction-limited objects of mNG was quantitated for three FOVs at each time point. Using the Ring TIRF illuminator ensures very flat TIRF illumination and image collection over much of the imaged area; however, image fields were restricted to identical confluent plan areas for each of the FOVs.

Immunofluorescence staining and colocalization analysis

Cells grown on glass coverslips were incubated with cetuximab at 37°C, fixed in freshly prepared 4% PFA for 15 min, permeabilized in 0.1% Triton X-100 in calcium- and magnesium-free (CMF)-PBS/0.1% BSA for 5 min, and then incubated for 1 h at RT with Alexa Fluor 488-conjugated goat antihuman IgG secondary antibodies (1:1,000) and mouse EEA.1 mAb (1:500) in CMF-PBS/0.1% BSA. EEA.1 antibody was detected using cyanine 3-conjugated donkey antimouse secondary antibody (1:500). Finally, samples were washed and mounted in ProLong Gold antifade reagent (Invitrogen) and 3D imaged through 488-nm and 561-nm laser channels using a spinning-disk confocal microscopy system. To quantify the amount of cetuximab-occupied EGFR localized in early endosomes (EEA.1-positive), 3D images of cetuximab-incubated cells were used to generate a segment mask to select EEA.1 endosomes detected through the 561-nm channel (EEA.1 mask). Another segment mask was generated with the minimum threshold to include total cetuximab fluorescence detected through the 488-nm channel (cetuximab mask). For both masks, identical threshold parameters were used for all images. The sum fluorescence intensity of the 488-nm channel in the EEA.1 mask was divided by the sum fluorescence intensity of the 488-nm channel in the cetuximab mask in each image to calculate the fraction of total cellular EGFR located in EEA.1-containing endosomes per FOV, each depicting 6–15 cells.

Western blot analyses

For detection of protein expression in gene-edited cells and siRNA knockdowns, the cells grown in full media were washed with cold CMF-PBS and lysed in TGH buffer (1% Triton X-100, 10% glycerol, 50 mM Hepes, 2 mM EGTA, phosphatase and protease inhibitors) for 10 min at 4°C. The lysates were pre-cleared by centrifugation at 16,000 $\times g$ at 4°C for 10 min and denatured by heating in a sample buffer for 5 min at 95°C. To detect RAS and RAS fusion proteins, the lysates were separated by SDS-PAGE (12% polyacrylamide gels) and transferred to nitrocellulose paper. Western blotting was performed as described (Surve et al., 2019), and blots were imaged using an Odyssey scanner (LI-COR).

To measure MEK1/2 and ERK1/2 phosphorylation, cells were serum starved overnight. Upon stimulation with EGF, the cells were washed with cold CMF-PBS and lysed as described above. The lysates were electrophoresed on 4–15% Criterion TGX precast gels (Bio-Rad Laboratories). The blots were probed with antibodies against total and phosphorylated MEK1/2 and ERK1/2. Blots were imaged using an Odyssey scanner and quantitated using LI-COR software. MEK1/2 and ERK1/2 activities were calculated as the ratio of the amount of the phosphorylated protein to the amount of total protein normalized to the maximum value of phosphorylated/total protein ratios in each individual time course experiment.

¹²⁵I-EGF binding and internalization assays

Mouse receptor grade EGF was ¹²⁵I conjugated, and ¹²⁵I-EGF binding and internalization assays were performed as described (Sorkin and Duex, 2010). Briefly, the number of surface EGFRs was measured in confluent cells grown in 12-well plates by incubating with 20 ng/ml ¹²⁵I-EGF at 4°C for 1 h, followed by washes. The cells were solubilized in 1 N NaOH, and the amount of radioactivity was normalized to the amount of protein per well. The background signal was measured in the presence of 1 μg/ml unlabeled EGF. For internalization assays, confluent cells in 12-well plates were incubated with ¹²⁵I-EGF for 5–60 min at 37°C in the absence or presence of unlabeled EGF (125-fold excess to estimate the background binding). When indicated, cells were pretreated with DMSO or Dyngo-4a for 30 min in DMEM (without BSA), and ¹²⁵I-EGF was applied in the same media supplemented with 0.1% BSA. Endocytosis was stopped by washing with ice-cold DMEM, and surface-bound ¹²⁵I-EGF was stripped by 5-min incubation with ice-cold 0.2 M sodium acetate buffer (pH 2.8). Cells were then lysed in 1 N NaOH to determine the amount of internalized ¹²⁵I-EGF. After background subtraction, the amounts of surface and internalized ¹²⁵I-EGF per well and the ratio of internalized and surface ¹²⁵I-EGF were plotted against time.

Statistics

All statistical analyses were performed using GraphPad Prism software (GraphPad Software). For comparisons of two groups, an unpaired Student's *t* test was used. For multiple comparison analyses, one-way ANOVA followed by Tukey's or Fisher's least significant difference multiple comparison test was used. Differences were considered significant when the *P* value was <0.05, with the specific *P* values shown in the figures.

Online supplemental material

Fig. S1 depicts the characterization of the properties of gene-edited HeLa cells, including the comparison of cell surface EGFR levels. Fig. S2 demonstrates detection of the auto-fluorescence in endosomal compartments of parental HeLa cells. Fig. S3 shows effects of CHC siRNA and Dyngo-4a on the time course of ¹²⁵I-EGF binding and internalization in HeLa cells. Fig. S4 shows additional examples of TERCs.

Acknowledgments

We are grateful to Drs. Caplan, Hammond, Linstedt, and Weisz for generous gifts of reagents.

This study was supported by National Science Foundation Division Molecular and Cellular Biosciences grant 1715132 and by National Institutes of Health grants CA089151 and GM124186.

The authors declare no competing financial interests.

Author contributions: S. Surve: conceptualization, data curation, formal analysis, validation, investigation, visualization, methodology, writing – review and editing; S.C. Watkins: investigation, software, review and editing; A. Sorkin: conceptualization, formal analysis, supervision, funding acquisition, visualization, validation, project administration, writing – review and editing.

Submitted: 16 July 2021

Revised: 21 August 2021

Accepted: 24 August 2021

References

- Bivona, T.G., and M.R. Philips. 2003. Ras pathway signaling on endomembranes. *Curr. Opin. Cell Biol.* 15:136–142. [https://doi.org/10.1016/S0955-0674\(03\)00016-4](https://doi.org/10.1016/S0955-0674(03)00016-4)
- Bivona, T.G., S.E. Quatela, B.O. Bodemann, I.M. Ahearn, M.J. Soskis, A. Mor, J. Miura, H.H. Wiener, L. Wright, S.G. Saba, et al. 2006. PKC regulates a farnesyl-electrostatic switch on K-Ras that promotes its association with Bcl-XL on mitochondria and induces apoptosis. *Mol. Cell.* 21: 481–493. <https://doi.org/10.1016/j.molcel.2006.01.012>
- Buday, L., P.H. Warne, and J. Downward. 1995. Downregulation of the Ras activation pathway by MAP kinase phosphorylation of Sos. *Oncogene.* 11: 1327–1331.
- Castellano, E., and E. Santos. 2011. Functional specificity of ras isoforms: so similar but so different. *Genes Cancer.* 2:216–231. <https://doi.org/10.1177/1947601911408081>
- Chiu, V.K., T. Bivona, A. Hach, J.B. Sajous, J. Silletti, H. Wiener, R.L. Johnson II, A.D. Cox, and M.R. Philips. 2002. Ras signalling on the endoplasmic reticulum and the Golgi. *Nat. Cell Biol.* 4:343–350. <https://doi.org/10.1038/ncb783>
- Day, C.A., N.W. Baetz, C.A. Copeland, L.J. Kraft, B. Han, A. Tiwari, K.R. Drake, H. De Luca, D.J.F. Chinnappen, M.W. Davidson, et al. 2015. Microtubule motors power plasma membrane tubulation in clathrin-independent endocytosis. *Traffic.* 16:572–590. <https://doi.org/10.1111/tra.12269>
- DeGraff, J.L., A.W. Gagnon, J.L. Benovic, and M.J. Orsini. 1999. Role of arrestins in endocytosis and signaling of α₂-adrenergic receptor subtypes. *J. Biol. Chem.* 274:11253–11259. <https://doi.org/10.1074/jbc.274.16.11253>
- Di Guglielmo, G.M., P.C. Baass, W.J. Ou, B.I. Posner, and J.J. Bergeron. 1994. Compartmentalization of SHC, GRB2 and mSOS, and hyperphosphorylation of Raf-1 by EGF but not insulin in liver parenchyma. *EMBO J.* 13:4269–4277. <https://doi.org/10.1002/j.1460-2075.1994.tb06747.x>
- Farmer, T., S. Xie, N. Naslavsky, J. Stöckli, D.E. James, and S. Caplan. 2021. Defining the protein and lipid constituents of tubular recycling endosomes. *J. Biol. Chem.* 296:100190.
- Fortian, A., and A. Sorkin. 2014. Live-cell fluorescence imaging reveals high stoichiometry of Grb2 binding to the EGF receptor sustained during endocytosis. *J. Cell Sci.* 127:432–444. <https://doi.org/10.1242/jcs.137786>
- Galperin, E., and A. Sorkin. 2008. Endosomal targeting of MEK2 requires RAF, MEK kinase activity and clathrin-dependent endocytosis. *Traffic.* 9:1776–1790. <https://doi.org/10.1111/j.1600-0854.2008.00788.x>
- Galperin, E., V.V. Verkhusha, and A. Sorkin. 2004. Three-chromophore FRET microscopy to analyze multiprotein interactions in living cells. *Nat. Methods.* 1:209–217. <https://doi.org/10.1038/nmeth720>
- Hammond, G.R.V., and J.E. Burke. 2020. Novel roles of phosphoinositides in signaling, lipid transport, and disease. *Curr. Opin. Cell Biol.* 63:57–67. <https://doi.org/10.1016/j.ceb.2019.12.007>
- Hood, F.E., B. Klinger, A.U. Newlaczyl, A. Sieber, M. Dorel, S.P. Oliver, J.M. Coulson, N. Blüthgen, and I.A. Prior. 2019. Isoform-specific Ras signaling is growth factor dependent. *Mol. Biol. Cell.* 30:1108–1117. <https://doi.org/10.1091/mbc.E18-10-0676>
- Howe, C.L., J.S. Valletta, A.S. Rusnak, and W.C. Mobley. 2001. NGF signaling from clathrin-coated vesicles: evidence that signaling endosomes serve

- as a platform for the Ras-MAPK pathway. *Neuron*. 32:801–814. [https://doi.org/10.1016/S0896-6273\(01\)00526-8](https://doi.org/10.1016/S0896-6273(01)00526-8)
- Hu, Y., W. Lu, G. Chen, P. Wang, Z. Chen, Y. Zhou, M. Ogasawara, D. Trachootham, L. Feng, H. Pelicano, et al. 2012. K-ras^{G12V} transformation leads to mitochondrial dysfunction and a metabolic switch from oxidative phosphorylation to glycolysis. *Cell Res*. 22:399–412. <https://doi.org/10.1038/cr.2011.145>
- Huang, F., A. Khvorova, W. Marshall, and A. Sorkin. 2004. Analysis of clathrin-mediated endocytosis of epidermal growth factor receptor by RNA interference. *J. Biol. Chem*. 279:16657–16661. <https://doi.org/10.1074/jbc.C400046200>
- Jiang, X., and A. Sorkin. 2002. Coordinated traffic of Grb2 and Ras during epidermal growth factor receptor endocytosis visualized in living cells. *Mol. Biol. Cell*. 13:1522–1535. <https://doi.org/10.1091/mbc.01-11-0552>
- Johannessen, L.E., T. Ringerike, J. Molnes, and I.H. Madhus. 2000. Epidermal growth factor receptor efficiently activates mitogen-activated protein kinase in HeLa cells and Hep2 cells conditionally defective in clathrin-dependent endocytosis. *Exp. Cell Res*. 260:136–145. <https://doi.org/10.1006/excr.2000.5004>
- Johnson, L., D. Greenbaum, K. Cichowski, K. Mercer, E. Murphy, E. Schmitt, R.T. Bronson, H. Umanoff, W. Edelmann, R. Kucherlapati, et al. 1997. K-ras is an essential gene in the mouse with partial functional overlap with N-ras. *Genes Dev*. 11:2468–2481. <https://doi.org/10.1101/gad.11.19.2468>
- Karnoub, A.E., and R.A. Weinberg. 2008. Ras oncogenes: split personalities. *Nat. Rev. Mol. Cell Biol*. 9:517–531. <https://doi.org/10.1038/nrm2438>
- Kawamoto, T., J.D. Sato, A. Le, J. Polikoff, G.H. Sato, and J. Mendelsohn. 1983. Growth stimulation of A431 cells by epidermal growth factor: identification of high-affinity receptors for epidermal growth factor by an anti-receptor monoclonal antibody. *Proc. Natl. Acad. Sci. USA*. 80:1337–1341. <https://doi.org/10.1073/pnas.80.5.1337>
- Lake, D., S.A. Corrêa, and J. Müller. 2016. Negative feedback regulation of the ERK1/2 MAPK pathway. *Cell. Mol. Life Sci*. 73:4397–4413. <https://doi.org/10.1007/s00018-016-2297-8>
- Lemmon, M.A., and J. Schlessinger. 2010. Cell signaling by receptor tyrosine kinases. *Cell*. 141:1117–1134. <https://doi.org/10.1016/j.cell.2010.06.011>
- Lu, A., F. Tebar, B. Alvarez-Moya, C. López-Alcalá, M. Calvo, C. Enrich, N. Agell, T. Nakamura, M. Matsuda, and O. Bachs. 2009. A clathrin-dependent pathway leads to KRas signaling on late endosomes en route to lysosomes. *J. Cell Biol*. 184:863–879. <https://doi.org/10.1083/jcb.200807186>
- Lynch, S.J., H. Snitkin, I. Gumper, M.R. Philips, D. Sabatini, and A. Pellicer. 2015. The differential palmitoylation states of N-Ras and H-Ras determine their distinct Golgi subcompartment localizations. *J. Cell. Physiol*. 230:610–619. <https://doi.org/10.1002/jcp.24779>
- Mandic, R., C.J. Rodgarkia-Dara, L. Zhu, B.J. Folz, M. Bette, E. Weihe, A. Neubauer, and J.A. Werner. 2006. Treatment of HNSCC cell lines with the EGFR-specific inhibitor cetuximab (Erbix) results in paradox phosphorylation of tyrosine 1173 in the receptor. *FEBS Lett*. 580:4793–4800. <https://doi.org/10.1016/j.febslet.2006.07.064>
- Misaki, R., M. Morimatsu, T. Uemura, S. Waguri, E. Miyoshi, N. Taniguchi, M. Matsuda, and T. Taguchi. 2010. Palmitoylated Ras proteins traffic through recycling endosomes to the plasma membrane during exocytosis. *J. Cell Biol*. 191:23–29. <https://doi.org/10.1083/jcb.200911143>
- Oksvold, M.P., E. Skarpen, B. Lindeman, N. Roos, and H.S. Huitfeldt. 2000. Immunocytochemical localization of Shc and activated EGF receptor in early endosomes after EGF stimulation of HeLa cells. *J. Histochem. Cytochem*. 48:21–33. <https://doi.org/10.1177/002215540004800103>
- Omerovic, J., D.E. Hammond, M.J. Clague, and I.A. Prior. 2008. Ras isoform abundance and signalling in human cancer cell lines. *Oncogene*. 27:2754–2762. <https://doi.org/10.1038/sj.onc.1210925>
- Pinilla-Macua, I., and A. Sorkin. 2015. Methods to study endocytic trafficking of the EGF receptor. *Methods Cell Biol*. 130:347–367. <https://doi.org/10.1016/bs.mcb.2015.05.008>
- Pinilla-Macua, I., S.C. Watkins, and A. Sorkin. 2016. Endocytosis separates EGF receptors from endogenous fluorescently labeled HRas and diminishes receptor signaling to MAP kinases in endosomes. *Proc. Natl. Acad. Sci. USA*. 113:2122–2127. <https://doi.org/10.1073/pnas.1520301113>
- Pol, A., M. Calvo, and C. Enrich. 1998. Isolated endosomes from quiescent rat liver contain the signal transduction machinery. Differential distribution of activated Raf-1 and Mek in the endocytic compartment. *FEBS Lett*. 441:34–38. [https://doi.org/10.1016/S0014-5793\(98\)01517-8](https://doi.org/10.1016/S0014-5793(98)01517-8)
- Prior, I.A., and J.F. Hancock. 2012. Ras trafficking, localization and compartmentalized signalling. *Semin. Cell Dev. Biol*. 23:145–153. <https://doi.org/10.1016/j.semcdb.2011.09.002>
- Prior, I.A., F.E. Hood, and J.L. Hartley. 2020. The frequency of Ras mutations in cancer. *Cancer Res*. 80:2969–2974. <https://doi.org/10.1158/0008-5472.CAN-19-3682>
- Ran, F.A., P.D. Hsu, J. Wright, V. Agarwala, D.A. Scott, and F. Zhang. 2013. Genome engineering using the CRISPR-Cas9 system. *Nat. Protoc*. 8:2281–2308. <https://doi.org/10.1038/nprot.2013.143>
- Rebollo, A., D. Pérez-Sala, and C. Martínez-A. 1999. Bcl-2 differentially targets K-, N-, and H-Ras to mitochondria in IL-2 supplemented or deprived cells: implications in prevention of apoptosis. *Oncogene*. 18:4930–4939. <https://doi.org/10.1038/sj.onc.1202875>
- Roy, S., B. Wyse, and J.F. Hancock. 2002. H-Ras signaling and K-Ras signaling are differentially dependent on endocytosis. *Mol. Cell Biol*. 22:5128–5140. <https://doi.org/10.1128/MCB.22.14.5128-5140.2002>
- Schlaepfer, D.D., S.K. Hanks, T. Hunter, and P. van der Geer. 1994. Integrin-mediated signal transduction linked to Ras pathway by GRB2 binding to focal adhesion kinase. *Nature*. 372:786–791. <https://doi.org/10.1038/372786a0>
- Schmick, M., N. Vartak, B. Papke, M. Kovacevic, D.C. Truxius, L. Rossmannek, and P.I.H. Bastiaens. 2014. KRas localizes to the plasma membrane by spatial cycles of solubilization, trapping and vesicular transport. *Cell*. 157:459–471. <https://doi.org/10.1016/j.cell.2014.02.051>
- Sharma, M., S.S. Giridharan, J. Rahajeng, N. Naslavsky, and S. Caplan. 2009. MICAL-L1 links EHD1 to tubular recycling endosomes and regulates receptor recycling. *Mol. Biol. Cell*. 20:5181–5194. <https://doi.org/10.1091/mbc.e09-06-0535>
- Shi, T., M. Niepel, J.E. McDermott, Y. Gao, C.D. Nicora, W.B. Chrisler, L.M. Markillie, V.A. Petyuk, R.D. Smith, K.D. Rodland, et al. 2016. Conservation of protein abundance patterns reveals the regulatory architecture of the EGFR-MAPK pathway. *Sci. Signal*. 9:rs6. <https://doi.org/10.1126/scisignal.aaf0891>
- Simanshu, D.K., D.V. Nissley, and F. McCormick. 2017. RAS proteins and their regulators in human disease. *Cell*. 170:17–33. <https://doi.org/10.1016/j.cell.2017.06.009>
- Sorkin, A., and J.E. Duex. 2010. Quantitative analysis of endocytosis and turnover of epidermal growth factor (EGF) and EGF receptor. *Curr. Protoc. Cell Biol*. Chapter 15:Unit 15.14.
- Sorkin, A., M. McClure, F. Huang, and R. Carter. 2000. Interaction of EGF receptor and grb2 in living cells visualized by fluorescence resonance energy transfer (FRET) microscopy. *Curr. Biol*. 10:1395–1398. [https://doi.org/10.1016/S0960-9822\(00\)00785-5](https://doi.org/10.1016/S0960-9822(00)00785-5)
- Sousa, L.P., I. Lax, H. Shen, S.M. Ferguson, P. De Camilli, and J. Schlessinger. 2012. Suppression of EGFR endocytosis by dynamin depletion reveals that EGFR signaling occurs primarily at the plasma membrane. *Proc. Natl. Acad. Sci. USA*. 109:4419–4424. <https://doi.org/10.1073/pnas.1200164109>
- Surve, S.V., P.J. Myers, S.A. Clayton, S.C. Watkins, M.J. Lazzara, and A. Sorkin. 2019. Localization dynamics of endogenous fluorescently labeled RAF1 in EGF-stimulated cells. *Mol. Biol. Cell*. 30:506–523. <https://doi.org/10.1091/mbc.E18-08-0512>
- Teis, D., W. Wunderlich, and L.A. Huber. 2002. Localization of the MP1-MAPK scaffold complex to endosomes is mediated by p14 and required for signal transduction. *Dev. Cell*. 3:803–814. [https://doi.org/10.1016/S1534-5807\(02\)00364-7](https://doi.org/10.1016/S1534-5807(02)00364-7)
- Terrell, E.M., D.E. Durrant, D.A. Ritt, N.E. Sealover, E. Sheffels, R. Spencer-Smith, D. Esposito, Y. Zhou, J.F. Hancock, R.L. Kortum, et al. 2019. Distinct binding preferences between Ras and Raf family members and the impact on oncogenic Ras signaling. *Mol. Cell*. 76:872–884.e5. <https://doi.org/10.1016/j.molcel.2019.09.004>
- Tycko, B., C.H. Keith, and F.R. Maxfield. 1983. Rapid acidification of endocytic vesicles containing asialoglycoprotein in cells of a human hepatoma line. *J. Cell Biol*. 97:1762–1776. <https://doi.org/10.1083/jcb.97.6.1762>
- Umanoff, H., W. Edelmann, A. Pellicer, and R. Kucherlapati. 1995. The murine N-ras gene is not essential for growth and development. *Proc. Natl. Acad. Sci. USA*. 92:1709–1713. <https://doi.org/10.1073/pnas.92.5.1709>
- Várnai, P., and T. Balla. 1998. Visualization of phosphoinositides that bind pleckstrin homology domains: calcium- and agonist-induced dynamic changes and relationship to myo-[³H]inositol-labeled phosphoinositide pools. *J. Cell Biol*. 143:501–510. <https://doi.org/10.1083/jcb.143.2.501>
- Vieira, A.V., C. Lamaze, and S.L. Schmid. 1996. Control of EGF receptor signaling by clathrin-mediated endocytosis. *Science*. 274:2086–2089. <https://doi.org/10.1126/science.274.5295.2086>
- Whistler, J.L., and M. von Zastrow. 1999. Dissociation of functional roles of dynamin in receptor-mediated endocytosis and mitogenic signal transduction. *J. Biol. Chem*. 274:24575–24578. <https://doi.org/10.1074/jbc.274.35.24575>

- Widmann, C., S. Gibson, M.B. Jarpe, and G.L. Johnson. 1999. Mitogen-activated protein kinase: conservation of a three-kinase module from yeast to human. *Physiol. Rev.* 79:143–180. <https://doi.org/10.1152/physrev.1999.79.1.143>
- Wiechmann, S., P. Maisonneuve, B.M. Grebbin, M. Hoffmeister, M. Kaulich, H. Clevers, K. Rajalingam, I. Kurinov, H.F. Farin, F. Sicheri, et al. 2020. Conformation-specific inhibitors of activated Ras GTPases reveal limited Ras dependency of patient-derived cancer organoids. *J. Biol. Chem.* 295:4526–4540. <https://doi.org/10.1074/jbc.RA119.011025>
- Wolfman, J.C., S.M. Planchon, J. Liao, and A. Wolfman. 2006. Structural and functional consequences of c-N-Ras constitutively associated with intact mitochondria. *Biochim. Biophys. Acta.* 1763:1108–1124. <https://doi.org/10.1016/j.bbamcr.2006.07.015>
- Yan, J., S. Roy, A. Apolloni, A. Lane, and J.F. Hancock. 1998. Ras isoforms vary in their ability to activate Raf-1 and phosphoinositide 3-kinase. *J. Biol. Chem.* 273:24052–24056. <https://doi.org/10.1074/jbc.273.37.24052>
- Yoshida, T., I. Okamoto, T. Okabe, T. Iwasa, T. Satoh, K. Nishio, M. Fukuoka, and K. Nakagawa. 2008. Matuzumab and cetuximab activate the epidermal growth factor receptor but fail to trigger downstream signaling by Akt or Erk. *Int. J. Cancer.* 122:1530–1538. <https://doi.org/10.1002/ijc.23253>

Supplemental material

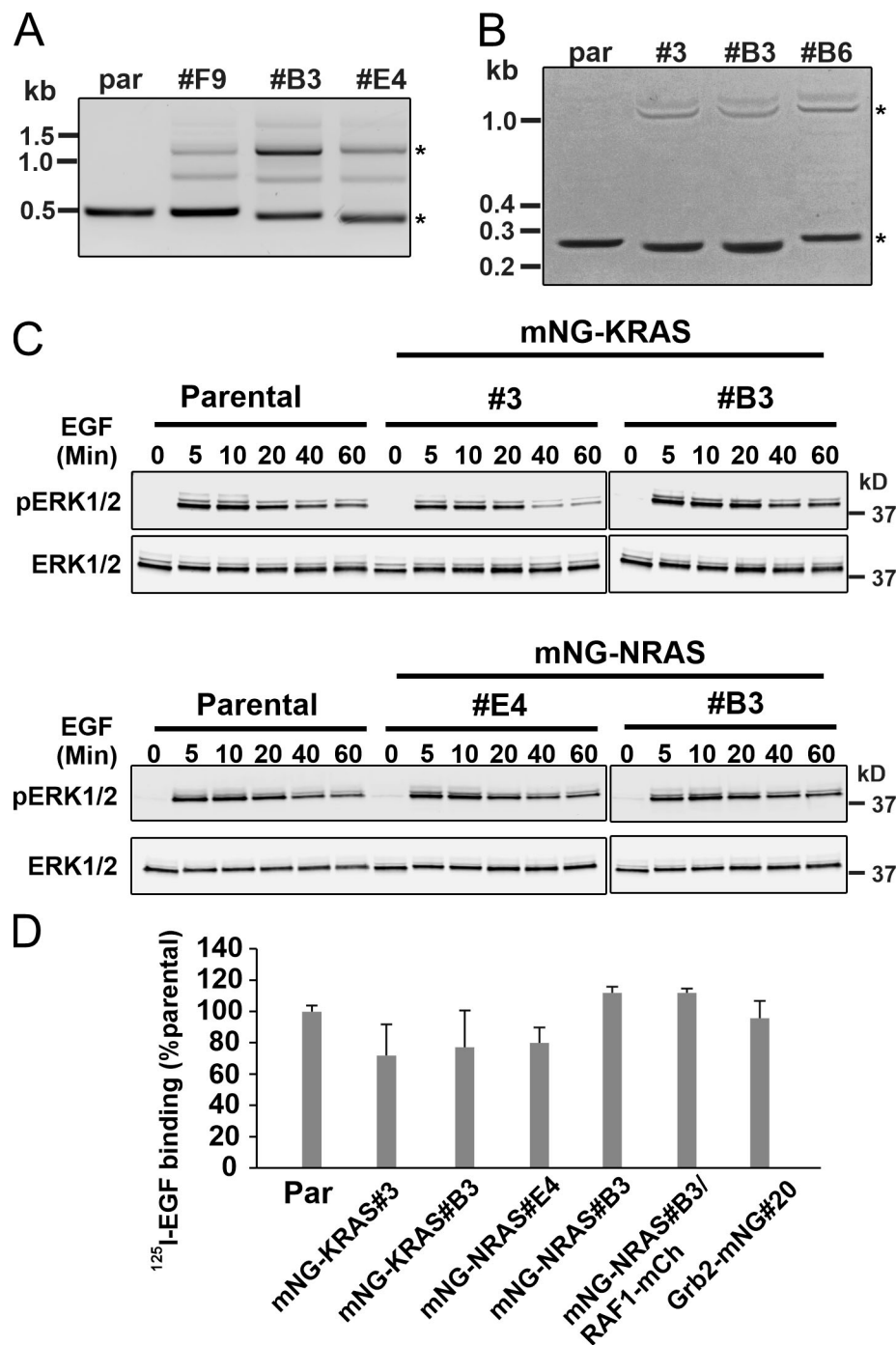


Figure S1. **Characterization of HeLa/mNG-KRAS and HeLa/mNG-NRAS cells and the comparison of surface EGFR levels in gene-edited HeLa cell clones.** (A and B) Genomic DNAs from parental and gene-edited HeLa cells were isolated using the Wizard genomic DNA purification kit (Promega). 100–200 ng of genomic DNA was used for the PCRs. (A) Genomic DNAs amplified using primers NrasutrF1 and NrasR2 (Table 1). Expected size of a single PCR product is 535 bp and 1,270 bp in parental and homozygous clones, respectively, and two amplicons of 535 and 1,270 bp in heterozygous clones. (B) Genomic DNAs amplified using primers KrasutrF1 and KrasR2 (Table 1). Expected size of a single PCR product was 280 bp and 1,015 bp in parental and homozygous clones, respectively, and two amplicons of 280 and 1,270 bp in heterozygous clones. Bands of interest are marked by asterisks. (C) Representative Western blots out of three experiments used to compare ERK1/2 activity in parental HeLa and tagged cell lines in Fig. 1. Parental HeLa, HeLa/mNG-KRAS, and HeLa/mNG-NRAS cells were serum starved and treated with 4 ng/ml EGF for 0–60 min at 37°C. Cell lysates were electrophoresed and probed by Western blotting with pERK1/2 and total ERK1/2 antibodies. (D) Binding of ¹²⁵I-EGF to parental and gene-edited HeLa cell clones. Confluent serum-starved cells grown in 12-well dishes were incubated with 20 ng/ml ¹²⁵I-EGF at 4°C for 1 h, and the amount of cell-associated radioactivity was measured as described in Materials and methods. Bar graphs represent mean cpm values with SDs (n = 3–6) normalized to that value in parental HeLa cells (parental cells have ~50,000 ¹²⁵I-EGF binding sites per cell).

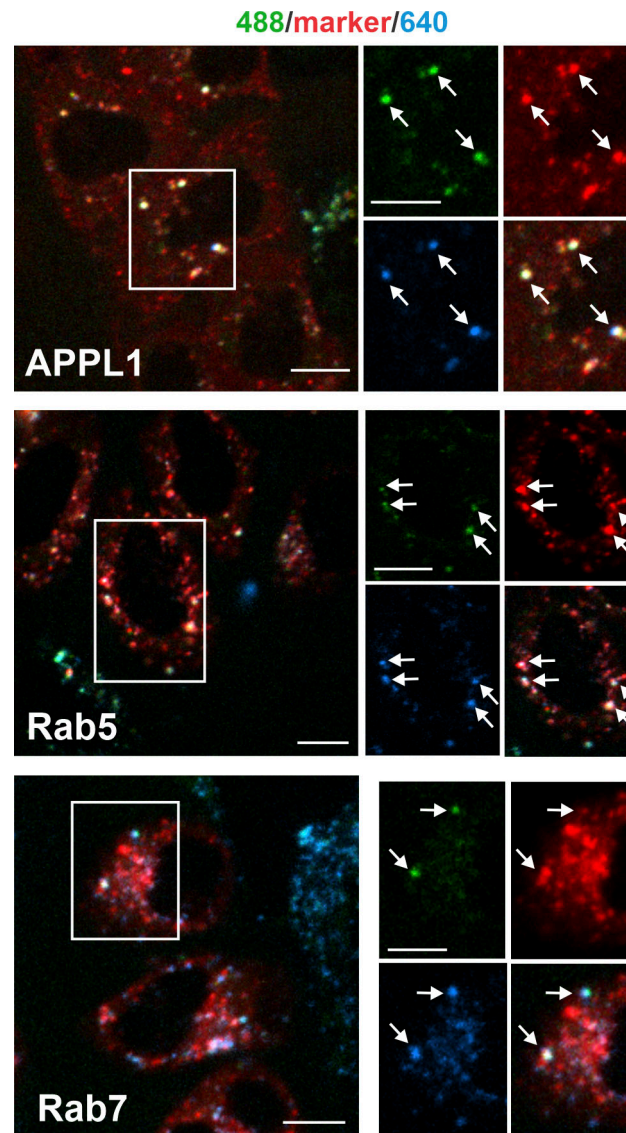


Figure S2. **Live-cell imaging of parental HeLa and endosomal markers.** HeLa cells were transfected with plasmids expressing mRFP-APPL1, mRFP-Rab5, and CFP-Rab7. 3 d after transfection, the cells were imaged through 488-nm (green), 561-nm (red; mRFP), 445-nm (red; CFP), and 640-nm (blue; auto-fluorescence) channels using image acquisition parameters identical to those used in Figs. 2 and 3. Merged-channel maximum-intensity z-projections of two or three consecutive confocal images are presented. Insets represent high-magnification/contrast split-channel images of the regions marked by white rectangles. Arrows point to examples of vesicles with signals from three channels (nonspecific colocalization). Autofluorescence through 561-nm and 445-nm channels was negligible with image acquisition parameters used for detection of corresponding endosomal markers; therefore, fluorescence through these channels is considered to be specific. Scale bars, 10 μ m.

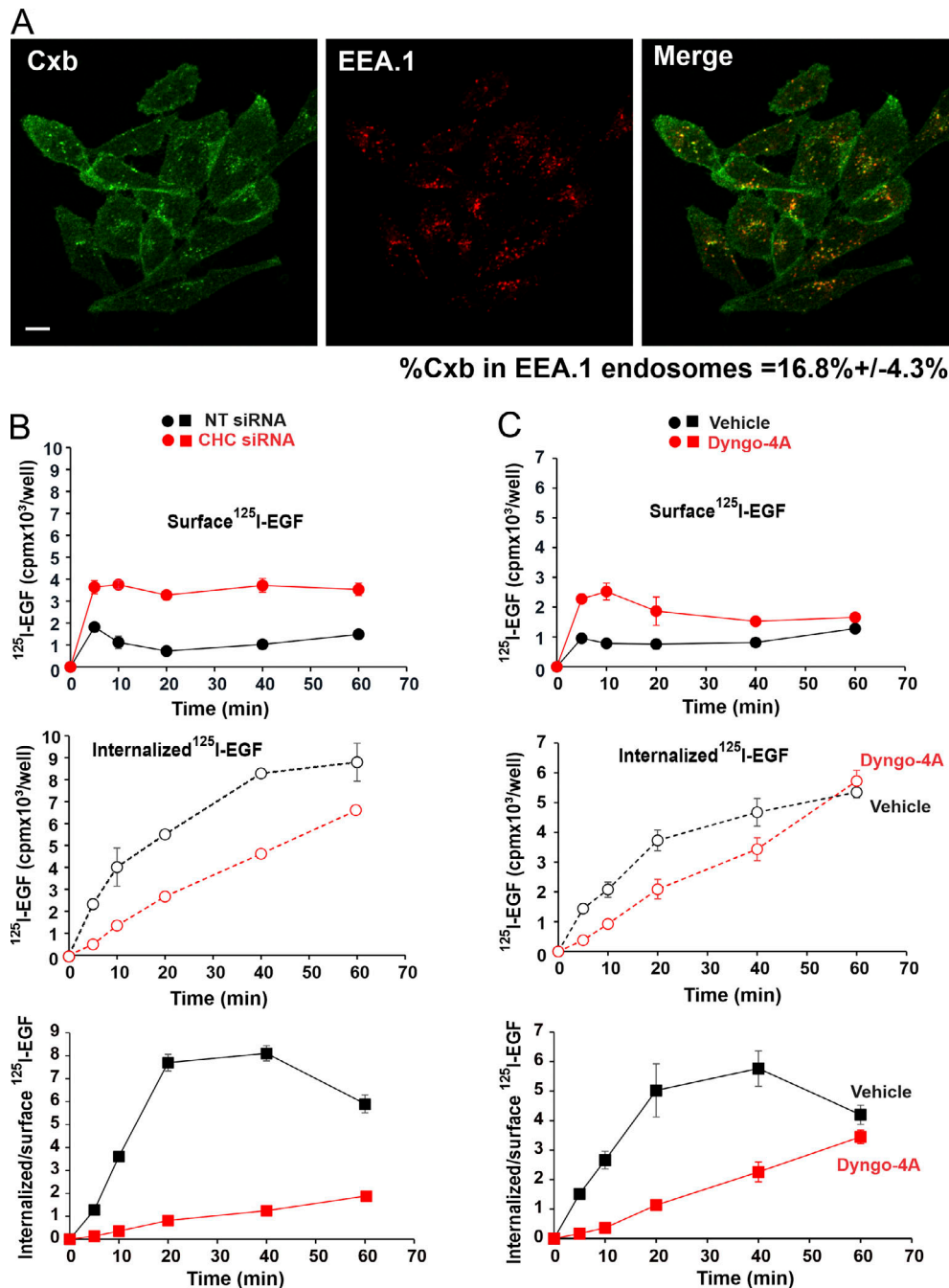


Figure S3. Effects of cetuximab, CHC siRNA, and Dyngo-4a on EGFR endocytosis. (A) Serum-starved parental HeLa cells were stimulated with 1 ng/ml EGF for 15 min and incubated with 5 μ g/ml cetuximab (Cxb) for an additional 15 min at 37°C followed by fixation and detection of cetuximab-occupied EGFRs by antihuman secondary antibodies conjugated with Alexa Fluor 488. Cells were colabeled with EEA.1 antibody detected by antimouse cyanine 3-conjugated secondary antibody. 3D images were acquired through the 488-nm (green; cetuximab) and 561-nm (red; EEA.1) channels. Representative single confocal section images are shown to demonstrate predominantly plasma membrane fluorescence of cetuximab and some vesicular colocalization with EEA.1. Scale bar, 10 μ m. Calculation of the percentage fractionation of total cell-associated cetuximab colocalized with EEA.1 was performed as described in Materials and methods. Mean value of the percentage fractionation with SDs ($n = 12$ fields of view) is indicated under the images. (B) Cells transfected with nontargeting (NT) or CHC siRNAs were incubated with 125 I-EGF for 5–60 min at 37°C. Surface-bound and internalized 125 I-EGF were measured. Background-subtracted amounts of surface and internalized 125 I-EGF per well and the ratio of internalized and surface 125 I-EGF were calculated and plotted against time. Each data point is a mean value of a duplicate with SDs. SDs are not visible if they are smaller than markers. Note that the amount of internalized 125 I-EGF in NT transfected cells may be underestimated due to fast endocytosis leading to 125 I-EGF lysosomal degradation. (C) Cells were pretreated with DMSO or Dyngo-4a for 30 min in DMEM (without BSA), and 125 I-EGF was applied in the same media supplemented with 0.1% BSA. Surface-bound and internalized 125 I-EGF were measured. Background-subtracted amounts of surface and internalized 125 I-EGF per well and the ratio of internalized and surface 125 I-EGF were calculated and plotted against time. Each data point is a mean value of a duplicate with SDs, except for a 60-min point, which is averaged from quadruplicates. SDs are not visible if they are smaller than markers. Note that the amount of internalized 125 I-EGF in vehicle-treated cells may be underestimated due to fast endocytosis leading to 125 I-EGF lysosomal degradation.

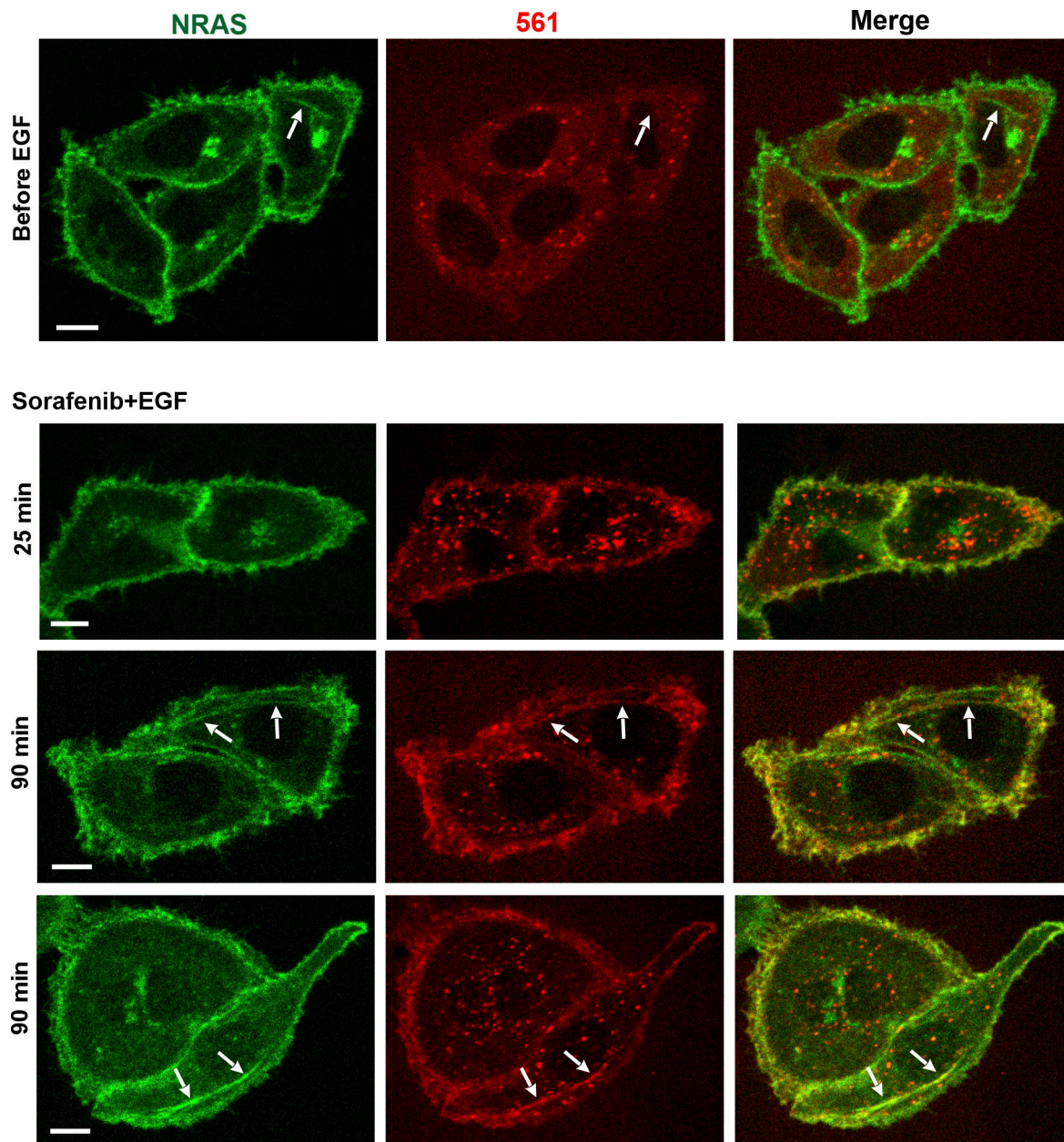


Figure S4. **Recruitment of endogenous RAF1-mCh to mNG-NRAS-labeled plasma membrane and TERC in double-gene-edited cells (additional to Fig. 9).** Live HeLa/mNG-NRAS/RAF1-mCh cells were imaged at 37°C before and after stimulation with 4 ng/ml EGF and sorafenib (10 μ M) through 488-nm (green; mNG) and 561-nm (red; mCh) channels. Maximum-intensity z-projections of two consecutive confocal images are shown. Arrows point to examples of colocalization of RAF1-mCh and mNG-NRAS in TERCs. Scale bars, 10 μ m.